Antitumor and Radiosensitizing Effects of Zinc Oxide-Caffeic Acid Nanoparticles against Solid Ehrlich Carcinoma in Female Mice

Hayam M. Sayed, MSc[1], Mahmoud M. Said, PhD[2], Nadia Y. S. Morcos, PhD[2], Mona A. El Gawish, PhD[1], and Amel F. M. Ismail, PhD[3] (iD)

Abstract

This study aimed to evaluate the anticancer and radio-sensitizing efficacy of Zinc Oxide-Caffeic Acid Nanoparticles (ZnO-CA NPs). ZnO-CA NPs were formulated by the conjugation of Zinc Oxide nanoparticles (ZnO NPs) with caffeic acid (CA) that were characterized by Fourier Transform Infrared Spectra (FT-IR), X-ray Diffractometer (XRD), and Transmission Electron Microscopy (TEM). In vitro anticancer potential of ZnO-CA NPs was evaluated by assessing cell viability in the human breast (MCF-7) and hepatocellular (HepG2) carcinoma cell lines. In vivo anticancer and radio-sensitizing effects of ZnO-CA NPs in solid Ehrlich carcinoma-bearing mice (EC mice) were also assessed. Treatment of EC mice with ZnO-CA NPs resulted in a considerable decline in tumor size and weight, down-regulation of B-cell lymphoma 2 (BCL2) and nuclear factor kappa B (NF-κB) gene expressions, decreased vascular cell adhesion molecule 1 (VCAM-1) level, downregulation of phosphorylated-extracellular-regulated kinase 1 and 2 (p-ERK1/2) protein expression, DNA fragmentation and a recognizable peak at sub-G_0/G_1 indicating dead cells' population in cancer tissues. Combined treatment of ZnO-CA NPs with γ-irradiation improved these effects. In conclusion: ZnO-CA NPs exhibit in-vitro as well as in-vivo antitumor activity, which is augmented by exposure of mice to γ-irradiation. Further explorations are warranted previous to clinical application of ZnO-CA NPs.

Introduction

Cancerous tumors are the foremost reasons for morbidity and mortality, considering that millions of peoples are dying annually. Breast cancer (BC) is categorized at the top of the most prevalent tumor types,[1] while hepatocellular carcinoma (HCC) is the fifth most widespread malignant tumor worldwide.[2] Quite a lot of basic modalities are used to manage cancerous tumors, either alone or combined, including chemotherapy (CT) and radiotherapy (RT). However, the effectiveness and application of CT and RT are hindered by their serious side effects.[3] Chemotherapeutic drugs show inadequate clinical effectiveness, due to the development of drug resistance during CT alongside the serious and life-threatening side-effects, which increases the mortality rate in cancer patients.[4] To deal with these problems, progress in new strategies is indispensable. Scientists continuously attempt to discover novel medications from natural phytoconstituents,[5] or synthetic/semisynthetic organic or inorganic compounds.[6-8]

A short time ago, nanotechnology took on the challenge of cancer treatment via fabrication of drugs in the nano-scale of 1-100 nm.[9] Radioresistance of tumor cells, as well as deterioration of normal cells are the shortcomings of RT. Accordingly, the radiosensitizers emerged as an important hot spot in the radiation oncology field.[10] Radiosensitizers are agents that

[1]Radiation Biology Department, National Center for Radiation Research and Technology, Egyptian Atomic Energy Authority, Cairo, Egypt
[2]Biochemistry Department, Faculty of Science, Ain Shams University, Cairo, Egypt
[3]Drug Radiation Research Department, National Center for Radiation Research and Technology, Egyptian Atomic Energy Authority, Cairo, Egypt

Corresponding Author:
Amel F. M. Ismail, Drug Radiation Research Department, National Center for Radiation Research and Technology, Egyptian Atomic Energy Authority, Ahmed El-Zomor St. 3, El-Zohoor District, Nasr City 11787, Cairo, Egypt.
Email: afmismail@gmail.com

can drive tumor cells to be sensitive to radiation via enhancing the liberation of free radicals, thus forcing the cells toward apoptosis.[11,12]

Metal-incorporated nanoparticles demonstrate chemical benefits, evincing synergistic cell-damaging consequences in radiation therapy.[10] According to Food and Drug Administration (FDA), Zinc Oxide nanoparticles (ZnO NPs) have emerged as a promising potent development in the medical field, particularly in cancer applications, due to their minor toxicity to healthy human cells.[13,14] ZnO NPs exhibit in vivo protective activities in rats and mice,[15,16] suggesting their safety for mammalian tissues. At the same time, ZnO NPs demonstrate in vitro anticancer activities,[17] inciting cytotoxicity in a cell-specific and proliferation-dependent approach.[18] ZnO NPs have specific characteristic features, including generation of the reactive oxygen species (ROS), which triggers mitochondria-mediated apoptosis. The hydroxyl radicals (OH^-), perhydroxyl radicals (HO_2^-), and superoxide anions (O_2^{-}), which are released from the surface of ZnO characterize the main constituents of ZnO NPs-cytotoxicity.[19] To potentiate biological activities, ZnO NPs were modified via green synthesis using a natural products extract,[20,21] doped with metal ions,[22] fabricated with natural products,[23,24] or loaded with antitumor agents such as doxorubicin[25] and paclitaxel.[26] Moreover, ZnO NPs were conjugated with caffeic acid.[27-29] Caffeic acid (CA, 3,4-dihydroxyphenyl-2-propenoic acid or 3,4-dihydroxycinnamic acid, $C_9H_8O_4$; molecular weight (M.wt) 180.16) is a near molecular analog of dihydroxyphenylalanine (DOPA).[27] CA is a natural phytochemical phenolic constituent in plants found in high concentrations in coffee, wine, and tea as well as in propolis. CA exhibits antioxidant and free radical scavenging properties, due to its rich chemical structure of phenolic-hydroxyls;[30,31] accordingly, it exhibits various biological functions, comprising antibacterial, anti-inflammatory, immunomodulatory, and anticancer activities.[32,33]

Accordingly, ZnO NPs were conjugated with CA to prepare ZnO-CA NPs to improve their in vitro antitumor activity. Moreover, the in vivo radiosensitizing and antitumor activities of ZnO-CA NPs were evaluated in an animal tumor model.

Material and Methods

Chemicals

Caffeic acid [$C_9H_8O_4$, M.wt: 180.16) and Zinc acetate [$Zn(CH_3CO_2)_2$, $ZnC_4H_6O_4$ with a M.wt: 183.48] were purchased from Sigma-Aldrich Chemical Co. (St. Louis, Mo, USA).

Preparation of Zinc Oxide Nanoparticles

Zinc Oxide NPs were fabricated as described previously with minor modification.[34] Briefly, Zinc acetate was stirred in de-ionized water (2% wt/volume) at $25 \pm 5°C$, for 30 to 60 minutes. Then, 1 mL of absolute acetic acid was added with continuous stirring for another 30 minutes. Then, a volume of 15 mL sodium hydroxide (NaOH, 5 M) was added to adjust the pH to 10-11. The produced white precipitate was rinsed with de-ionized H_2O to obtain neutral pH (7.0), then filtered to collect the ZnO NPs, which were left to dry.

Preparation of Zinc Oxide-Caffeic Acid Nanoparticles

Caffeic acid was conjugated with the prepared ZnO NPs at a molar ratio of 1:1 in absolute ethanol (EtOH) solution to prepare ZnO–CA NPs. Briefly, 0.180 g CA (1 mmol) was stirred in 100 mL absolute ethanol for 5 minutes and mixed with 0.081 g ZnO NPs that were added slowly with continuous stirring (1–2 hours, at $25 \pm 5°C$) in the dark. The grayish-yellow solid product was collected and rinsed with cold absolute EtOH to remove the residual reactants. The resultant ZnO-CA NPs were dried under vacuum overnight.

Characterizations of Zinc Oxide-Caffeic Acid Nanoparticles

X-ray diffraction (XRD). The diffraction patterns of the prepared ZnO NPs and ZnO-CA NPs were recorded with Philip's PW1390 X'Pert Pro X-ray Diffractometer (The PANalytical Organization, Almelo, Netherlands) with Ni-filtered Cu Kα radiation at a 40 kV generator voltage and 0.154 nm wavelength, at $25 \pm 5°C$. The diffraction angle 2θ checked at a rate of 2° minutes⁻¹. The diffractometer was operated automatically under constant operating conditions.[35]

Transmission electron microscopy (TEM). The morphology of ZnO NPs, and ZnO-CA NPs was characterized by a JEM-100 CX Transmission Electron Microscopy (TEM) (JEOL Ltd., Tokyo, Japan) at the National Center for Radiation Research and Technology (NCRRT, Cairo, Egypt).

Fourier transform infrared spectra (FT-IR). Caffeic acid, ZnO NPs, and ZnO-CA NPs FT-IR spectra were recorded in the range of 400 to 4000 cm⁻¹, at $25 \pm 5°C$. The analysis was carried out using AIT Matson Infinity Series Equipment Model 960 M0009, 4 cm⁻¹ resolution (Triad Scientific, New Jersey, USA).

Determination of the median lethal dose (LD_{50}) of Zinc Oxide-Caffeic Acid Nanoparticles. The median lethal dose (LD_{50}) of ZnO-CA NPs was assessed by the intraperitoneal injection of increasing concentrations from the prepared compound in female mice, according to Akhila et al.[36] The compound was given to 6 animals per dose. The number of deaths and signs of clinical toxicity were recorded. The animals were observed for all physiologic signs before dosing and for all signs of toxicity 48 hours after dosing. One-tenth of the

LD$_{50}$ value has been used as an ideal dose to determine the in-vivo antitumor activity of the investigated compounds.

Human equivalent dose (HED) of Zinc Oxide-Caffeic Acid Nanoparticles. According to the method of Nair and Jacoub,[37] drug doses were converted from animal studies to human studies by the body surface area (BSA) normalization method.

$$HED\,(mg/Kg) = (Animal\,NOAL\,mg/Kg)$$
$$\times Animal\,K_m\,/\,Human\,\,K_m$$

Where NOAL is No observed adverse effect level, Km = Weight in Kg/Body surface area

Evaluation of the In Vitro Cytotoxicity of Zinc Oxide-Caffeic Acid Nanoparticles against Human Breast Cancer MCF-7 and Human Hepatocellular Adenocarcinoma HepG2 Cell Lines

The cytotoxicity of CA, ZnO NPs, and ZnO-CA NPs against human breast cancer MCF-7 and human hepatocellular adenocarcinoma HepG2 cell lines after 48 hours was determined using the MTT cell viability assay. As designated previously,[38] cells were plated in a flat-bottom 96-well microtiter plate, treated with different concentrations of the tested compounds and incubated for 48 hours in a humidified atmosphere at 37°C and 5% CO$_2$. After the incubation period, 10 µl of MTT solution (0.5 mg/mL) was added to each well and incubated for 4 hours. A volume of 100 µl from the solubilizing solution was added into each well. The plate was allowed to stand overnight and then was checked for complete solubilization of the formazan crystal. The absorbance was measured spectrophotometrically at 590 nm. Three independent experiments were conducted.

Experimental Animals

Seventy-two outbred female Swiss albino mice (25-35 g) were obtained from the Egyptian Organization for Biological Products and Vaccines (Cairo, Egypt). They were distributed in 6 groups (n = 12), in specially-designed plastic cages, under healthy circumstances at 25 + 5°C, with 12 hours dark/light phases accompanied by suitable pressure, humidity, and good ventilation. Animals were fed the available animal pellet diet (20%-23% protein) with continuous drinking water *ad-libitum*. All animal procedures were carried out following the International Standards for the experimental animals, and approved by the NCRRT Ethical Committee (20A/21).

Radiation Exposure

The animals were subjected to gamma-irradiation from Canadian Gamma Cell-40 with [137]Cesium source (Atomic Energy of a Canada Ltd., Ontario, Canada) at the NCRRT, Egyptian Atomic Energy Authority, at a dose rate of 0.45 Gy/min. The animal's whole body was exposed to 2 Gy/week for 3 successive doses, a total of 6 Gy/anima according to Abdallah et al.[12]

Tumor Transplantation

Ehrlich ascites carcinoma (EAC) murine cells, which were kindly given by the National Cancer Institute (NCI, Cairo University, Egypt), were transmitted by weekly intraperitoneal (IP) injection of Ehrlich carcinoma (EC) cells into the mice at the NCRRT. Then, 2.5×10^6 viable EC cells were inoculated intramuscularly into the right thigh of the lower limb of each female mouse to create solid EC tumors.[39] The tumor length and width were measured at the end of the third and fourth weeks following Ehrlich's ascites cells inoculation, using a vernier caliper; subsequently, tumor volume could be computed by the equation: Tumor volume(cm^3) = ½(length × width^2),[40] where the largest longitudinal diameter is the length and the largest transverse diameter is the width.

Experimental Design

The 72 adult female mice were arbitrarily distributed equally into 6 groups of 12, as follows:

- **Group 1 (Control, C):** Mice without any treatment left for 4 consecutive weeks.
- **Group 2 (ZnO-CA):** Mice injected intraperitoneally (IP) with ZnO-CA NPs (5 mg/100 g bw, 1/10 LD$_{50}$) every other day for 3 consecutive weeks.
- **Group 3 (Ehrlich, E):** Mice-bearing EC tumor left for 4 consecutive weeks.
- **Group 4 (E + R):** One week following solid EC tumor inoculation, animals were subjected to 2 Gy of whole-body γ-irradiation /week for 3 consecutive weeks to 6 Gy total.
- **Group 5 (E + ZnO-CA):** One week following solid EC tumor inoculation, mice were injected intraperitoneally (IP) with ZnO-CA NPs (5 mg/100 g bw) every other day for 3 consecutive weeks.
- **Group 6 (E + ZnO-CA + R):** One week following solid EC tumor inoculation, mice were injected intraperitoneally (IP) with ZnO-CA NPs (5 mg/100 g bw) every other day along with 2 Gy whole-body γ-irradiation /week for 3 consecutive weeks.

After an overnight fasting period, all the mice were anesthetized with diethyl ether at the end of 3 successive weeks of tumor treatment; the blood was collected by heart puncture and separated into 2 parts. The first part was collected in EDTA tubes, to quantify the hematologic indices. The

second part was collected in glass tubes and left to coagulate for 15 minutes at 37°C, then the serum was separated after centrifugation at 1200 ×*g*, and stored at −20°C for biochemical analysis.

At autopsy, the solid tumors of different groups and the right thigh of the lower limb of the control animals were dissected immediately, washed in sterile isotonic saline, dried on a filter paper, and conserved at −80°C. Likewise, parts of specimens were fixed in 10% formalin for histopathological consideration.

Biochemical Analysis

Different hematological parameters (hemoglobin (Hb) concentration, red blood cells (RBCs), white blood cells (WBCs), and platelet (PLTs) counts) were assessed in the whole blood samples using a blood counter (BC-2800, Mindray, China). The serum alanine aminotransferase (ALT) and aspartate aminotransferase (AST) activities, as well as creatinine concentrations were analyzed using commercial kits provided by Spinreact (Spain), whereas serum urea level was assayed using a commercial kit supplied by Diamond Diagnostics (Egypt).

RNA Extraction and Real Time Quantitative Polymerase Chain Reaction (qRT-PCR)

Parts of the solid tumor (groups 3-6) and the right thigh of the lower limb (groups 1 and 2) from animals were used for the determination of B-cell lymphoma 2 (BCL2) and nuclear factor kappa B (NF-κB) gene expression. RNeasy® Mini kit (Qiagen, Germany) was used to obtain the total RNA from the tissue samples as specified by the manufacturer's instructions, reverse transcribed into complementary DNA (cDNA) by Thermo Scientific™ RevertAid™ First Strand cDNA Synthesis Kit (Fermentus, Thermo Fisher Scientific Inc, UK), and then amplified using quantitative real-time polymerase chain reaction (qRT-PCR), in a thermal cycler (ABI PRISM 7500 Fast Sequence Detection System, USA), using Power SYBR® Green PCR Master Mix (Applied Biosystems, USA). The following thermal cycling conditions were used: 95°C for 10 minutes, subsequently, 40 cycles of 95°C for 15 s, finally 60°C for 1 minute. The sequence of PCR primer pairs and gene bank accession numbers were as follows; B-Cell Lymphoma 2 (BCL2) (NM_009741.5): F: 5′-GTG GTG GAG GAA CTC TTC AG- 3′, R: 5′ GTT CCA CAA AGG CAT CCC AG-3′,[41] Nuclear Factor-Kappa B (NF-κB) (NM_008689.2): F: 5′-GAA ATT CCT GAT CCA GAC AAA AAC-3′, R: 5′-ATC ACT TCA ATG GCC TCT GTG TAG-3′ and glyceraldehyde 3-phosphate dehydrogenase (GAPDH), (NM_008084), F: 5′-ATG TGT CCG TCG TGG ATC TGA C-3′, R: 5′-AGA CAA CCT GGT CCT CAG TGT AG-3′.[42] The obtained data were examined, handling the ABI Prism sequence detection system software, then computed by PE Biosystems

(Foster City, CA) v1•7 Sequence Detection Software. Using the proportional threshold cycle technique, the genes' relative expression ratios were assessed and standardized to the GAPDH gene. The expression $2^{-\Delta\Delta Ct}$ was applied to quantify the final relative ratios.[43]

Western Blot Analysis of Phosphorylated-Extracellular-Regulated Kinase 1 and 2

A tissue sample (100 mg) was homogenized in 1.0 mL ice-cold RIPA lysing buffer and centrifuged at 16,000 *g* for 30 minutes at 4°C. The protein concentration was calculated in the separated supernatant using the Bradford Protein Assay Kit (BIO BASIC INC., Markham Ontario, Canada). Twenty micrograms of protein in each lane were screened with 10% SDS polyacrylamide gel electrophoresis, then transported to polyvinylidene fluoride membranes. The membrane was then incubated at room temperature for 2 hours with 5% bovine serum albumin in TBST blocking solution, then incubated with a phospho-ERK1/2 (Thr202, Tyro204) primary antibody solution (1/500) (Cat No: 14-9109-82, Invitrogen, USA) at 4°C overnight and thereafter rinsed 3 times with TBST buffer. Subsequently, the membrane was incubated with a secondary monoclonal antibody connected with horseradish peroxidase, at room temperature for 2 hours. A Clarity TM Western ECL chemiluminescent substrate (BIO-RAD, USA) was successively added to the membrane. The chemiluminescent signals were captured by a CCD camera. Image analysis software was used after standardization with β-actin on the Chemi Doc™ MP imager to measure the band strength of the phosphorylated-extracellular-regulated kinase (p-ERK1/2) protein expression against the control sample.

Determination of Vascular Cell Adhesion Molecule-1 Level

A mouse sandwich enzyme-linked immunosorbent assay (ELISA) kit (MyBioSource, Cat No. MBS2601120, USA) was used to calculate the concentration of vascular cell adhesion molecule-1 (VCAM-1) in the thigh muscles or tumor tissues.

DNA Fragmentation Assay

DNA fragmentation analysis was performed, using agarose gel electrophoresis.[44] Briefly, a small piece of the thigh muscle of the normal control mice or tumor tissues of different treated groups were incubated in Triton-Tris-EDTA (TTE) lysis buffer and proteinase-K overnight at 50°C; sodium chloride (4 M) was then added, and the tubes were shaken vigorously for 20 seconds, and centrifuged at 20000 ×g for 10 minutes, at 27°C. The supernatant was mixed with cold absolute ethanol (1:1 v/v). The samples were centrifuged and the DNA pellet was washed with 70% ethanol

then re-suspended in TE buffer. Equal volumes of DNA were mixed with the loading buffer and 10 μL was applied into each well of a 1% agarose gel. An appropriate DNA molecular weight marker of 100 to 1000 base pairs (M) (BIO BASIC INC, Markham, Ontario, Canada) was included. The electrophoresis was run in Tris Acetate EDTA (TAE) buffer containing bromophenol blue dye. To visualize DNA, the gel was placed on a UV transilluminator and photos of the gel were taken.

Analysis of Cell Cycle Progression by Flow Cytometry

Analysis of the cell cycle by flow cytometry was carried out according to the method of Givan.[45] Briefly, 0.1 g frozen right thigh muscle or solid EC tumor was homogenized in phosphate-buffered saline (PBS) and washed twice with PBS. After centrifugation, the cell pellets were re-suspended and incubated at room temperature for 30 minutes in 1 mL of propidium iodide (PI)/Triton X-100 staining solution (0.1% Triton X-100 in PBS, 0.2 mg/mL RNase A and 10 mg/mL PI). A MoFlo Flow Cytometer (MoFlo, DakoCytomation, Denmark) was used to examine the stained cells.

Histopathological Observation

Right thigh muscles and solid EC tumor tissue specimens were fixed in 10% formalin solution for at least 3 days at 4°C, then processed to form paraffin cubes. Thin sections (4-5 μm) were stained with hematoxylin and Eosin (H&E) solution and examined under a light microscope.[46]

Statistical Analysis

The Shapiro-Wilks normality test ($p > 0.05$) revealed that all data had been normally distributed. Using one-way analysis of variance (ANOVA), statistical analysis of the difference between means was carried out. In the case of a significant F-ratio, the multi-comparison post hoc Duncan test was used to evaluate the statistical significance among the treated groups at a significance level of $p < 0.05$. All the statistical analysis was performed using version 20.0 of the Statistical Package for Social Science (SPSS).

Results

Characterizations of Zinc Oxide Nanoparticles and Zinc Oxide-Caffeic Acid Nanoparticles

The X-ray diffraction peaks showed the nanocrystalline character and purity of ZnO NPs with hexagonal wurtzite structure. These peaks were at scattering angles (2θ) of 31.77, 34.40, 36.22, 47.50, 56.60, 62.63, 66.39, 67.95, 69.06, 72.56 and 76.97, which can designate diffraction from: 100, 002, 101, 102, 110, 103, 200, 112, 201, 004, and 202 crystal planes, respectively (Figure 1a). Similarly, the X-ray diffraction pattern of ZnO-CA NPs indicates that the product had a typical hexagonal wurtzite structure and no diffraction peaks of CA or other impurity phases were detected (Figure 1b).

A TEM scan of ZnO NPs showed a fully aggregated shape with a spherical structure and average particle size of approximately 30 nm (Figure 1c). Dis-similarly, ZnO-CA NPs exhibit the desegregation of ZnO NPs and absorption of CA on their surface. Spherical ZnO-CA NPs with approximately 23 nm size were noticed (Figure 1d).

FT-IR spectra of CA were identical, and contained absorption bands characteristic of phenol-carboxylic acids: 3431 and 3350 cm^{-1}ν(OH)arom, 3231 cm^{-1} ν(=C-H)arom, 3057, 3026, and 2988 cm^{-1}ν(CH) + ν(CH)C=C, 2837–2565 cm^{-1}ν(OH)acid, 1645 cm^{-1}ν(C=O), 1526 and 1451 cm^{-1}ν(CC), 1354 cm^{-1}ν(CC) + β(OH), 1279 cm^{-1}ν (C-OH), 1218 cm^{-1}β(OH) + β(CH)C=C, 1175 cm^{-1}β(CH), 1119 cm^{-1}β(CH), 972 γ(CH)C=C + γ(CH), 935 cm^{-1} γ(CH), 901 cm^{-1} ν(CCO), 851 cm^{-1} γ(CH), 816 cm^{-1} β (C=O), 780 cm^{-1} γ(CH), 736 cm^{-1} α(CCC), 698 cm^{-1}γ (C=O), 648 cm^{-1} β(C=O), 600 cm^{-1} γ(OH). The symbol "ν," "β," "γ," and "α (CCC)": indicate the stretching vibrations, in-plane bending modes, out-of-plane bending modes, and the aromatic ring in-plane bending modes, respectively (Figure 1e). The structural analysis of wurtzite ZnO nanoparticles was further verified through FT-IR exploration: 3393 cm^{-1} ν(O-H), 2876 cm^{-1} ν(CO$_2$), 1558 and 1507 and 1338 cm^{-1} ν(C=O), 829, 675, 52, and 471 cm^{-1} ν(Zn-O) (Figure 1f). The ZnO-CA NPs FT-IR spectra with the following signals: 3393, 3314 cm^{-1} ν(O-H), 3057, 3026, and 2988 cm^{-1}ν(CH) + ν(CH)C=C, 2880 cm^{-1} ν(CO$_2$), 1556 and 1510 cm^{-1} ν(C=O), 1269 cm^{-1}ν(C-OH), 1218 cm^{-1}β(OH) + β (CH)C=C, 1121 cm^{-1}β(CH), 972 γ(CH)C=C + γ(CH), 832 cm^{-1}, 675, 521, and 471 cm^{-1} ν(Zn-O) were noticed (Figure 1g).

Determination of the Median Lethal Dose (LD$_{50}$) of Zinc Oxide-Caffeic Acid Nanoparticles

The results revealed that the LD$_{50}$ value of ZnO-CA NPs is 50.0 mg/100 g bw (Table 1).

Human Equivalent Dose (HED) of Zinc Oxide-Caffeic Acid Nanoparticles

$$HED\,(mg/Kg) = (Animal\,NOAL\,mg/Kg)$$
$$\times Animal\,K_m / Human\,K_m.$$

From the results in Table 1: NOAL = 3 mg/Kg bw.

Km = Weight in Kg/Body surface area.
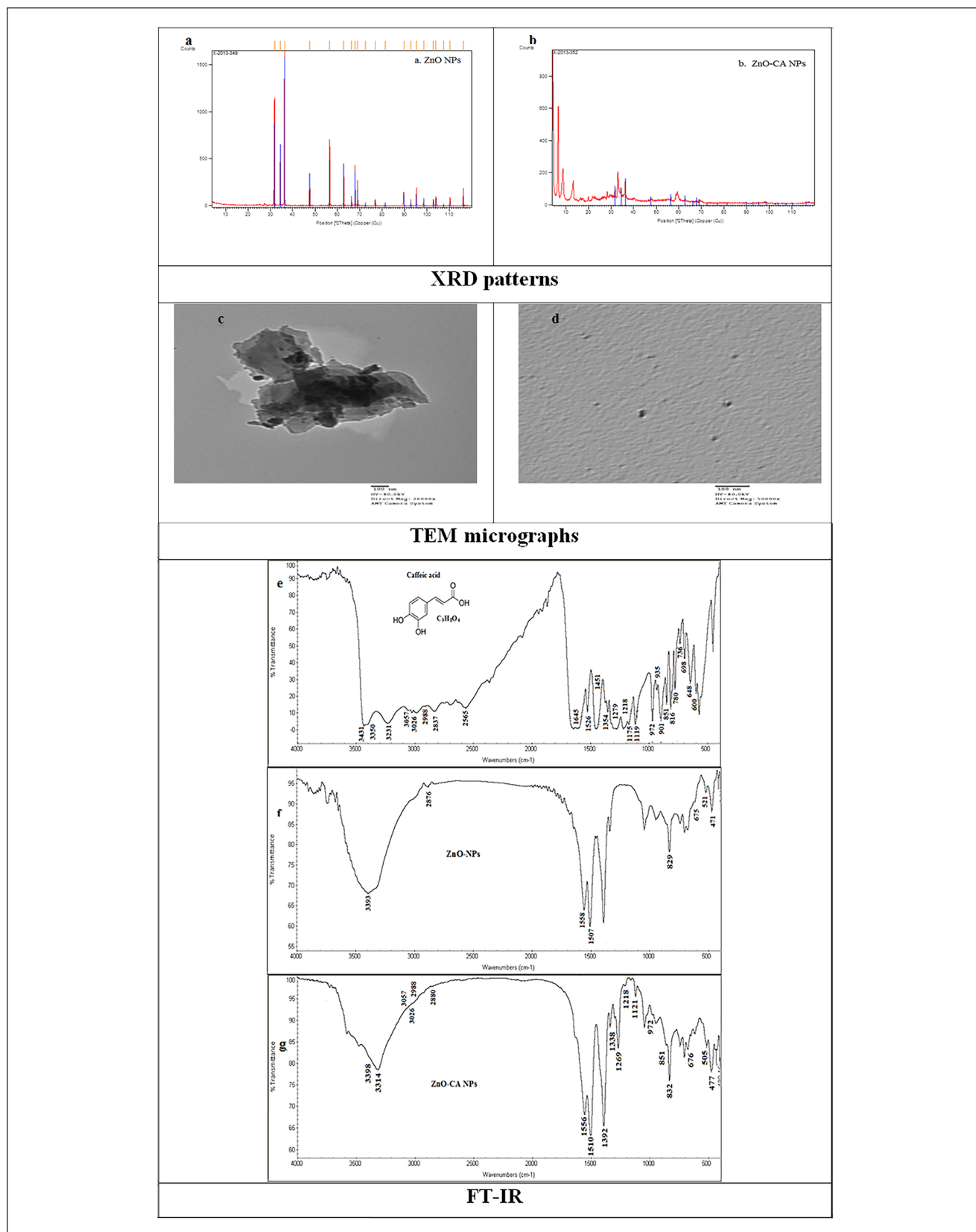The average mouse weight in this study is 30 gm and the body surface area is 0.01 m^2.[37]

Figure 1. Characterization of Zinc Oxide Nanoparticles, and Zinc Oxide–Caffeic Acid Nanoparticles.
Abbreviations: XRD: X-ray diffraction; TEM: transmission electron microscopy; FT-IR: Fourier-transform infrared spectroscopy.

Table 1. Determination of the Median Lethal Dose (LD_{50}) of Zinc Oxide-Caffeic Acid Nanoparticles in Female Mice.

Dose of ZnO-CA NPs (mg/100 g bw)	No. of mice	Survivors (S)	Deaths (D)	Mortality (%)
10	6	6	0	0
20	6	6	0	0
30	6	6	0	0
40	6	5	1	16.7
50	6	3	3	50.0
60	6	2	4	66.7

Abbreviation: bw, body weight.

Therefore, the K_m factor for mice is calculated by dividing 0.03 by 0.01.[37]

On the other hand, the average human body weight is 60 kg and the body surface area is 1.62 m². Therefore, the K_m factor for humans is calculated by dividing 60 by 1.62.[37]

Thus: Animal K_m = 0.03/0.01, Human K_m 60/1.62.

Accordingly, the Human Equivalent Dose of ZnO-CA NPs: HED = 0.243 mg/Kg.

In Vivo Toxicity and Mortality Study

During the experimental period (4 weeks), no mortality was recorded in normal control mice or those treated with ZnO-CA NPs as well as in EC solid tumor-bearing mice, either per se or those treated with ZnO-CA NPs. One female mouse out of 12 died (8.3% mortality) in animals bearing solid EC tumor that were either irradiated only or co-administered ZnO-CA NPs along with γ-irradiation.

In Vitro Cytotoxicity of Caffeic Acid, Zinc Oxide Nanoparticles, and Zinc Oxide-Caffeic Acid Nanoparticles against MCF7 and HepG2 Cells

The viability percentages (viability%) of the breast cancer (MCF7) and human hepatocellular adenocarcinoma HepG2 cell lines treated with different concentrations of CA, ZnO NPs, and ZnO-CA NPs were declined, however, their toxicity percentages (toxicity%) were enhanced in a dose-dependent manner, as demonstrated in Figure 2. The median growth inhibitory concentration (IC_{50}) values of CA, ZnO NPs, and ZnO-CA NPs were 38.23, 7.92, and 9.22 µg/mL for MCF7 cells, while, IC_{50} values of 50.02, 21.52, and 11.53 µg/mL were evaluated for HepG2 cells, respectively. Zinc Oxide NPs triggered higher toxicity% on MCF7 and HepG2 cancer cells, as compared to that obtained by CA. However, ZnO-CA NPs improved the toxicity% on HepG2 cancer cells, as compared to that obtained by ZnO NPs.

Tumor Volume and Weight

A considerable reduction ($p < 0.001$) in the tumor volume of solid EC-bearing mice treated with ZnO-CA NPs either alone (65.65% and 53.93%) or combined with γ-irradiation

(79.83% and 77.49%) was recorded at the third and fourth weeks, respectively, after inoculation of EC cells into the right thigh muscle of female mice, compared to untreated solid EC-bearing mice. Furthermore, a measurable reduction ($p < 0.001$) in the tumor weight was recorded in EC-bearing mice at sacrifice, either treated with ZnO-CA NPs alone (56.1%) or combined with γ-irradiation (71.9%), as compared to untreated solid EC-bearing mice (Table 2).

Biochemical Parameters and Hematology Indices

The data presented in Table 3 demonstrate that mice bearing solid EC tumors showed marked increments ($p < 0.001$) in serum AST and ALT activities (264.57% and 255.06%, respectively), compared to control mice. Treatment of solid EC-bearing mice with γ-irradiation resulted in significant declines in AST and ALT activities (15.28% and 24.74%, respectively), compared to untreated solid EC-bearing mice. Similarly, a considerable decline was observed in serum AST activity of solid EC-bearing mice treated with ZnO-CA NPs alone (10.17%) or combined with γ-irradiation (61.70%), as compared to untreated solid EC-bearing mice. Animals bearing solid EC tumors and treated with ZnO-CA NPs manifested a rebound to control serum ALT level, whereas a significant reduction in serum ALT was recorded (79.13%) in solid EC-bearing mice treated with both ZnO-CA NPs and γ-radiation, as compared to untreated solid EC-bearing mice. Also, exposure of solid EC-bearing mice to γ-irradiation resulted in a considerable rise ($p < 0.001$) in serum urea level (17.96%), compared to untreated solid EC-bearing mice. Similarly, treatment of solid EC-bearing mice with ZnO-CA NPs, alone or combined with γ-radiation, caused a considerable rise in serum urea level (40.38% and 29.42%, respectively), as compared to untreated solid EC-bearing mice. However, the serum creatinine level revealed a negligible change in the different treatment modalities. Normal mice treated with ZnO-CA NPs showed a slight significant decrease ($p < 0.001$) in Hb concentration (11.7%), while, a significant increase ($p < 0.001$) was observed in PLTs count (12.97%), as compared to control mice. Contrarily, mice bearing solid EC tumors demonstrated a considerable
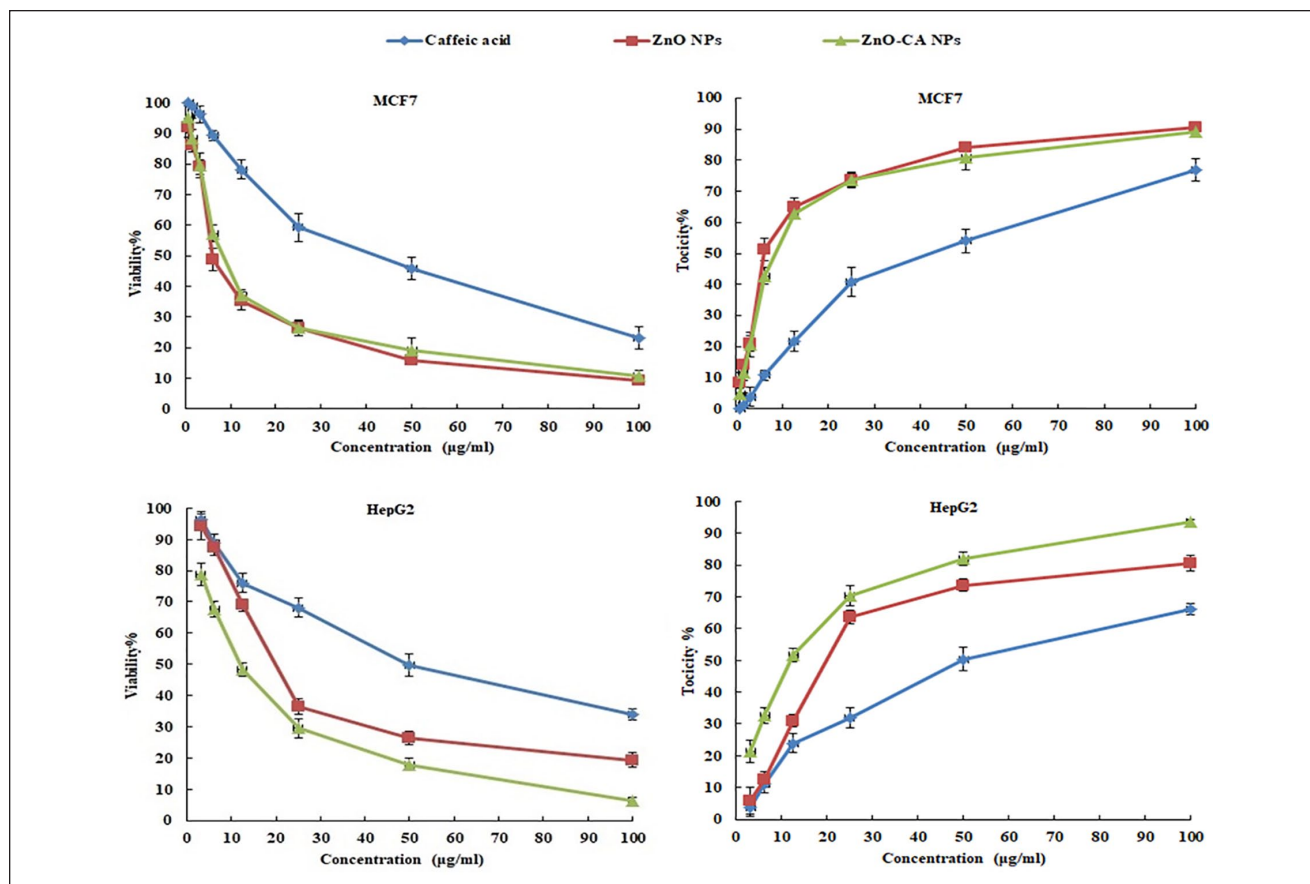
Figure 2. The Viability and Toxicity percentages of Breast cancer cell line (MCF7) and Human hepatocellular adenocarcinoma HepG2 cell lines treated with different concentrations of Caffeic Acid, Zinc Oxide Nanoparticles, and Zinc Oxide–Caffeic acid Nanoparticles. The median growth inhibitory concentration (IC_{50}) values of CA, ZnO NPs and ZnO-CA NPs were 38.23, 7.92, and 9.22 μg/mL for MCF7 cells, while, IC_{50} values for HepG2 cells were 50.02, 21.52, and 11.53 μg/mL, respectively.
Abbreviations: ZnO NPs: Zinc Oxide nanoparticles; ZnO-CA NPs: Zinc Oxide–Caffeic acid nanoparticles.

Table 2. Effect of γ-Radiation Exposure and/or Zinc Oxide–Caffeic Acid Nanoparticles Treatment on the Tumor Volume and Weight of Solid Ehrlich Bearing Mice.

	Tumor volume (cm³)		
Groups	Third week (21 days)	Fourth week (28 days)	Tumor weight (g)
E[#]			
Mean ± SE	1.19 ± 0.14[a]	1.91 ± 0.14[a]	5.7 ± 0.32[a]
E+R[@]			
Mean ± SE	1.13 ± 0.10[a]	1.6 ± 0.14[a]	5.3 ± 0.33[a]
% Change	−5.04	−16.23	−7.0
E+ZnO-CA[#]			
Mean ± SE	0.41 ± 0.06[b]	0.88 ± 0.14[b]	2.5 ± 0.16[b]
% Change	−65.55	−53.93	−56.1
E+ZnO-CA+R			
Mean ± SE	0.24 ± 0.04[b]	0.43 ± 0.07[c]	1.6 ± 0.12[c]
% Change	−79.83	−77.49	−71.9
F-ratio	25.13	28.62	66.24

Results are mean of 11-12 mice ± SE; [@]n = 11, and [#]n = 12 (one mouse out of 12 died in animals bearing solid Ehrlich (EC) tumor that were either irradiated only or co-administered ZnO-CA NPs along with gamma (γ)-irradiation). Values with dissimilar superscripts are significantly different. E: Solid EC bearing mice, R: mice exposed to 2 Gy of whole body γ-irradiation/week, for 3 consecutive weeks, and ZnO-CA: mice injected intraperitoneally with 5 mg/100 g body weight ZnO-CA NPs, every other day for 3 consecutive weeks. %Change versus E. *P*-value < 0.001.

Table 3. Effect of γ-Radiation Exposure and/or Zinc Oxide–Caffeic Acid Nanoparticles Treatment on Some Toxicity Parameters.

Parameters	C[#]	ZnO-CA[#]	E[#]	E+R[@]	E+ZnO-CA[#]	E+ZnO-CA+R[@]
AST (U/L)	429 ± 19.9^a	438 ± 22.29^a	1564 ± 47.89^b	1325 ± 88.30^c	1405 ± 6.97^c	599 ± 11.71^d
% Change		2.10	264.57	208.86	227.51	39.63
% Change*				−15.28	−10.17	−61.70
ALT (U/L)	247 ± 8.99^a	209 ± 11.26^{ad}	877 ± 32.89^b	660 ± 6.51^c	243 ± 6.57^a	183 ± 5.14^d
% Change		−15.38	255.06	167.21	−1.62	25.91
% Change*				−24.74	−72.29	−79.13
Urea (mg/dL)	27.90 ± 1.33^{ab}	25.50 ± 0.91^a	26.00 ± 0.78^a	30.67 ± 1.26^{bd}	36.50 ± 1.63^c	33.65 ± 0.89^{cd}
% Change		−8.60	−6.81	9.93	30.82	20.61
% Change*				17.96	40.38	29.42
Creatinine (mg/dL)	0.52 ± 0.02^a	0.51 ± 0.02^a	0.5 ± 0.03^a	0.48 ± 0.024^a	0.47 ± 0.021^a	0.51 ± 0.026^a
% Change		−1.92	−3.85	−7.69	−9.62	−1.92
% Change*				−4.00	−6.00	2.00
Hb% (g/dL)	14.7 ± 0.38^a	12.98 ± 0.36^b	11.4 ± 0.37^c	10.4 ± 0.49^c	10.9 ± 0.34^c	8.9 ± 0.5^d
% Change		−11.7	−22.45	−29.3	−25.85	−39.46
% Change*				−8.77	−4.39	−21.93
RBCs ($\times 10^{12}$/L)	7.5 ± 0.24^a	6.9 ± 0.24^{ab}	6.3 ± 0.2^{bc}	5.5 ± 0.25^d	5.6 ± 0.26^{cd}	4.6 ± 0.29^e
% Change		−8	−16.0	−26.67	−25.33	−38.67
% Change*				−12.7	−11.11	−26.98
WBCs ($\times 10^9$/L)	6.39 ± 0.40^a	5.68 ± 0.39^a	13.32 ± 0.29^b	2.16 ± 0.14^c	9.64 ± 0.10^d	2.69 ± 0.12^c
% Change		−10.93	108.45	−66.25	50.86	−57.90
% Change*				−83.78	−27.63	−79.80
PLTs ($\times 10^9$/L)	370.2 ± 3.48^a	418.5 ± 13.06^b	479.21 ± 12.93^c	380.08 ± 9.5^a	359.3 ± 9.55^a	300.0 ± 15.48^d
%Change		12.97	29.44	2.67	−2.94	−18.96
%Change*				−20.69	−25.02	−37.40

Results are mean of 11-12 mice ± SE. [@]n = 11, and [#]n = 12 (one mouse out of 12 died in animals bearing solid Ehrlich (EC) tumor that were either irradiated only or co-administered ZnO-CA NPs along with gamma (γ)-irradiation). Values with dissimilar superscripts are significantly different. C: control, E: Solid EC bearing mice, R: mice exposed to 2 Gy of whole body γ-irradiation/week, for 3 consecutive weeks, and ZnO-CA: mice injected intraperitoneally with 5 mg/100 g body weight ZnO-CA NPs, every other day for 3 consecutive weeks. %Change versus C and * %Change versus E. P-value < 0.001.

decline in Hb concentration and RBCs (22.45% and 16.0%, respectively), however, WBCs and PLTs counts were significantly increased ($p < 0.001$) (108.45% and 29.44%, respectively), as compared to control mice. Exposure of solid EC-bearing mice to γ-irradiation produced a significant decrease in RBCs, WBCs and PLTs counts (12.7%, 83.78%, and 20.69%, respectively), as compared to untreated EC-bearing mice. Also, ZnO-CA NPs treatment of solid EC-bearing mice normalized PLTs count and evinced a considerable decline in WBCs count (27.63%), as compared to untreated EC-bearing mice. In addition, solid EC-bearing mice treated with ZnO-CA NPs and γ-irradiation showed considerable declines of Hb concentration, RBCs, WBCs, and PLTs counts (21.93%, 26.98%, 79.80%, and 37.40%, respectively), as compared to untreated EC-bearing mice (Table 3).

Relative Gene Expression Ratios of B-Cell Lymphoma 2 (Bcl2) and Nuclear Factor Kappa B (NF-κB)

The inoculation of solid EC tumors in female mice caused a considerable up-regulation ($p < 0.001$) in the gene expression of tumor BCL2 and NF-κB (8.3 and 9.7 folds, respectively), compared to that of non-EC-bearing mice. On the other hand, solid EC-bearing mice exposed to γ-irradiation showed a considerable down-regulation in tumor BCL2 and NF-κB gene expression (53.03% and 44.63%, respectively), compared to untreated EC-bearing mice. Treatment of solid EC-bearing mice with ZnO-CA NPs alone or combined with γ-irradiation rebound BCL2 gene expression level to the control level, and induced a significant reduction in NF-κB (51.85% and 78.70%, respectively), compared to untreated EC-bearing mice (Figure 3).

Western Blot Analysis of Phosphorylated ERK1/2 Protein Expression

Western blot analysis of phosphorylated extracellular signal-regulated kinase 1 and 2 (p-ERK1/2) protein expression relative to β-actin was demonstrated in Figure 4A. The inoculation of solid EC into female mice caused a considerable up-regulation ($p < 0.001$) in tumor p-ERK1/2 protein expression (936.36%), as compared to non-EC-bearing mice. Exposure of solid EC-bearing mice to γ-irradiation produced a considerable down-regulation in p-ERK1/2
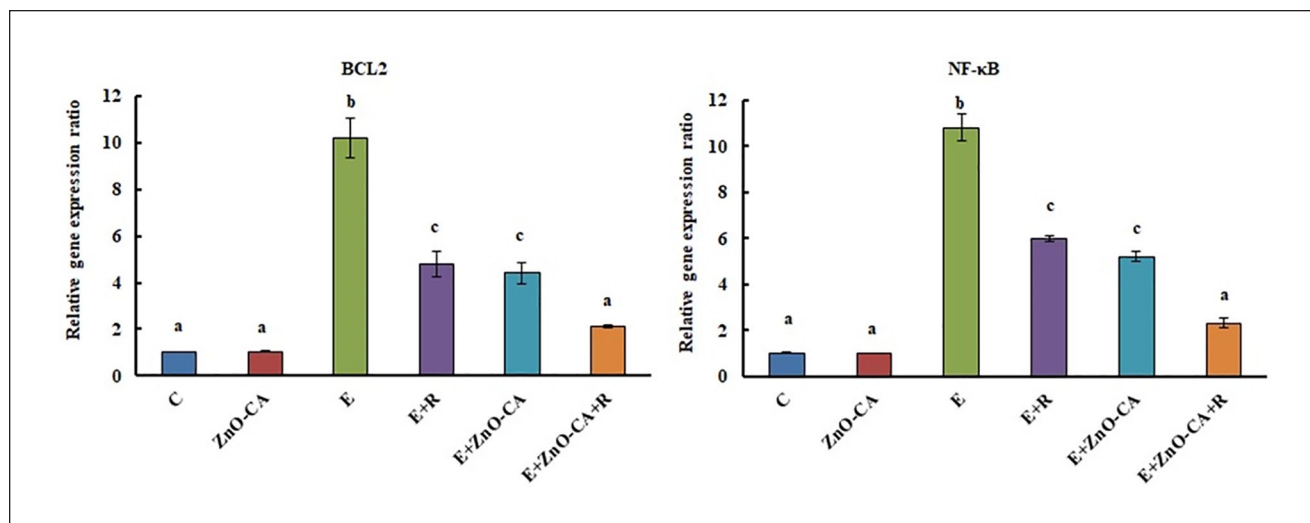
Figure 3. Effect of γ-Radiation Exposure and/or Zinc Oxide–Caffeic Acid Nanoparticles Treatment on the gene expression ratios of B-cell lymphoma 2 (BCL2) and Nuclear Factor- kappa B (NF-κB) relative to Glyceraldehyde 3-phosphate dehydrogenase (GAPDH). Results are mean of 6 mice ± SE. Values with dissimilar superscripts are significantly different. C: control, E: Solid Ehrlich (EC) bearing mice, R: mice exposed to 2 Gy of whole-body gamma (γ)-irradiation/week for 3 consecutive weeks, and ZnO-CA: Mice injected intraperitoneally with 5 mg of Zinc Oxide – Caffeic acid nanoparticles (ZnO-CA NPs)/100 g body weight, every other day for 3 consecutive weeks. Relative gene expression was measured in thigh muscle of non-EC bearing mice (C and ZnO-CA groups) or tumor tissues of solid EC bearing mice of different treated groups. P-value < 0.001.

protein expression (55.26%), as compared to untreated solid EC-bearing mice. Similarly, treatment of solid EC-bearing mice with ZnO-CA NPs alone or combined with γ-irradiation generated a considerable down-regulation in p-ERK1/2 level (57.89% and 74.56%, respectively), as compared to untreated solid EC-bearing mice (Figure 4B).

Vascular Cell Adhesion Molecule-1 (VCAM-1) level

The inoculation of solid EC in female mice initiated a considerable sharp increase ($p < 0.001$) in VCAM-1 level (666.66%) in the solid tumors, as compared to the intact muscular tissue of non-EC-bearing mice. Exposure to γ-irradiation triggered a significant decrease in VCAM-1 level (58.39%), as compared to untreated EC-bearing mice. Similarly, solid EC-bearing mice treated with ZnO-CA NPs along or combined with γ-irradiation gave rise to a considerable decline in the tumor VCAM-1 levels (52.17% and 73.91%, respectively), related to untreated solid EC-bearing mice (Figure 5).

DNA Fragmentation Pattern

DNA extracted from the thigh muscles of normal control mice (lane 2), and ZnO-CA NPs-treated mice (lane 3) or from the tumor tissue of untreated solid EC-bearing mice (lane 4), showed dense DNA bands without any fragmentation. By contrast, solid EC-bearing mice exposed to

γ-irradiation (lane 5), or treated with ZnO-CA NPs only (lane 6), or combined with γ-irradiation (lane 7) showed DNA damage, as evidenced by the appearance of DNA strand breaks (Figure 6).

Cell Cycle Analysis

Data of the cell cycle analysis presented in Table 4 and Figure 7 show a significant decrease ($P < 0.001$) in G0/G1 populations (39.23%), whereas a significant increase was recorded in S phase and G2/M populations (208.14% and 525.67%, respectively) in tumor tissues (E group), as compared to intact muscular tissue of non-EC-bearing mice. By contrast, solid EC-bearing mice exposed to γ-irradiation displayed a considerable increase in subG1 population (711.94%) accompanied by a considerable decrease in S phase, and G2/M populations (62.75% and 40.17%, respectively), as compared to untreated EC-bearing mice. Similarly, a considerable increase was recorded in subG1 population (617.1%), associated with a considerable decline in G0/G1, S phase, and G2/M populations (11.03%, 67.66%, and 46.72%, respectively) in the tumor tissue of solid EC-bearing mice treated with ZnO-CA NPs, compared to untreated EC-bearing mice. A more pronounced considerable increase was recorded in subG1 population (1187.1), concomitant with more considerable declines in G0/G1, S phase, and G2/M populations (19.47%, 81.47%. and 80.5%, respectively) in the tumor tissue of γ-irradiated and ZnO-CA NPs-treated mice, as compared to untreated EC-bearing mice.
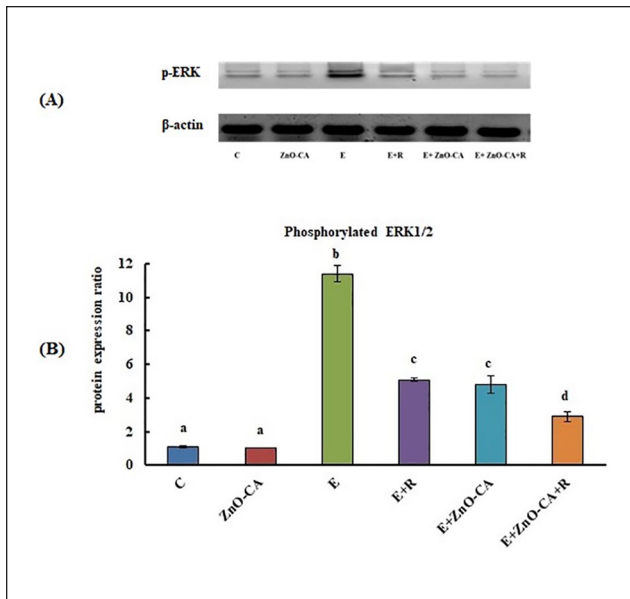
Figure 4. (A): Western blot analysis of phosphorylated extracellular signal-regulated kinase 1 and 2 (p-ERK1/2) protein expression relative to β-actin. (B): Effect of γ-Radiation Exposure and/or Zinc Oxide–Caffeic Acid Nanoparticles treatment on the phosphorylated extracellular signal-regulated kinase 1 and 2 (p-ERK 1/2) protein expression relative to β-actin in the thigh muscle (control) or tumor tissues.
Results are mean ± SE of 3 mice. Values with dissimilar superscripts are significantly different. C: control, E: Solid Ehrlich (EC) bearing mice, R: mice exposed to 2 Gy of whole-body gamma (γ)-irradiation/week for 3 consecutive weeks, and ZnO-CA: Mice injected intraperitoneally with 5 mg of Zinc Oxide–Caffeic acid nanoparticles (ZnO-CA NPs)/100 g bodyweight, every other day for 3 consecutive weeks. Relative gene expression was measured in thigh muscle of non EC bearing mice (C and ZnO-CA groups) or tumor tissues of solid EC bearing mice of different treated groups. P-value < 0.001.

Histopathological Investigations

The thigh muscles from control mice (Figure 8a) and ZnO-CA NPs-treated mice (Figure 8b) displayed normal histopathological configuration of striated bundles demonstrating normal muscular fibers. By contrast, solid EC tumors inoculated in the thigh muscle of an untreated mouse (Figure 8c) revealed massive numbers of intact anaplastic EC tumor cells implanted between skeletal muscle bundles and criteria of malignancy with minimum cellular necrosis. On the other hand, solid tumors from γ-irradiated EC-bearing mice (Figure 8d) demonstrated mild necrosis in the focal areas of the EC tumor. Also, ZnO-CA NPs-treated solid EC-bearing mice (Figure 8e) exhibited implanted EC tumor cells between skeletal muscle bundles, with moderate focal areas of necrosis. Moreover, solid EC tumors treated with ZnO-CA NPs and γ-irradiation (Figure 8f) exhibited wide severe focal necrotic areas.
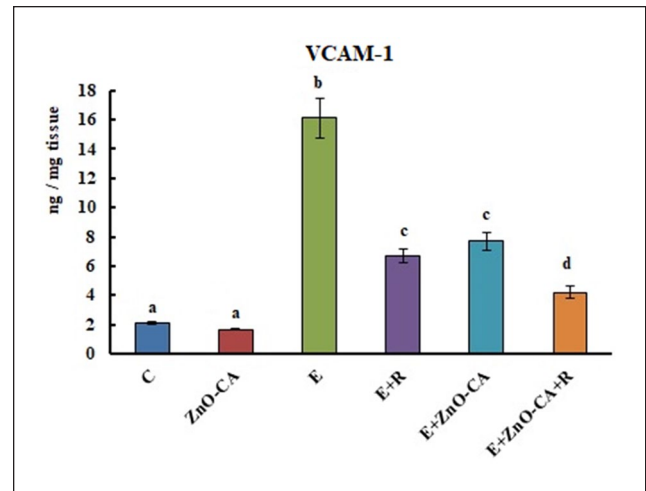

Figure 5. Effect of γ-Radiation Exposure and/or Zinc Oxide–Caffeic Acid Nanoparticles Treatment on the Vascular cell adhesion molecule 1 (VCAM-1) level.
Results are mean ± SE of 6 mice. Values with dissimilar superscripts are significantly different. C: control, E: Solid Ehrlich (EC) bearing mice, R: mice exposed to 2 Gy of whole-body gamma (γ)-irradiation/week for 3 consecutive weeks, and ZnO-CA: Mice injected intraperitoneally with 5 mg of Zinc Oxide–Caffeic acid nanoparticles (ZnO-CA NPs)/100 g bodyweight, every other day for 3 consecutive weeks. VCAM-1 level was measured in thigh muscle of non-EC bearing mice (C and ZnO-CA groups) or tumor tissues of solid EC bearing mice of different treated groups. P-value < 0.001.

Discussion

The X-ray diffraction peaks point out the nanocrystalline characters and purity of ZnO NPs with hexagonal wurtzite structure. The 2θ values matched with those of the standard hexagonal wurtzite structure ZnO as described earlier.[22,47] The diffraction peaks were more concentrated and narrower, suggesting that the nanostructures have the same crystalline character of ZnO materials.[48] Also, the sharp peak shows that there are large crystalline domains and a high degree of crystallinity in the nanostructures. In the XRD pattern, no unusual diffraction peaks were found, implying the nonexistence of other contaminations. The lack of any peaks associated with contaminations suggests that CA was correctly doped into the structure of ZnO NPs,[49] the TEM image revealed the absorption of CA on the surface of ZnO NPs as spherical nanoparticles with approximately 23 nm particle size.

FT-IR spectra of CA, handling KBr discs, revealed that the spectral assignments were carried out based on data from the literature.[28-30,50-52] The bands at: 3431 and 3350 cm^{-1} are appointed to –O–H stretching vibration of OH aromatic, 3231 cm^{-1} is appointed to =C–H stretching vibration of phenol ring, 3057, 3026, and 2988 cm^{-1} are appointed to C-H stretching vibration of phenol ring, 2837–2565 cm^{-1} are appointed to –O–H stretching vibration of
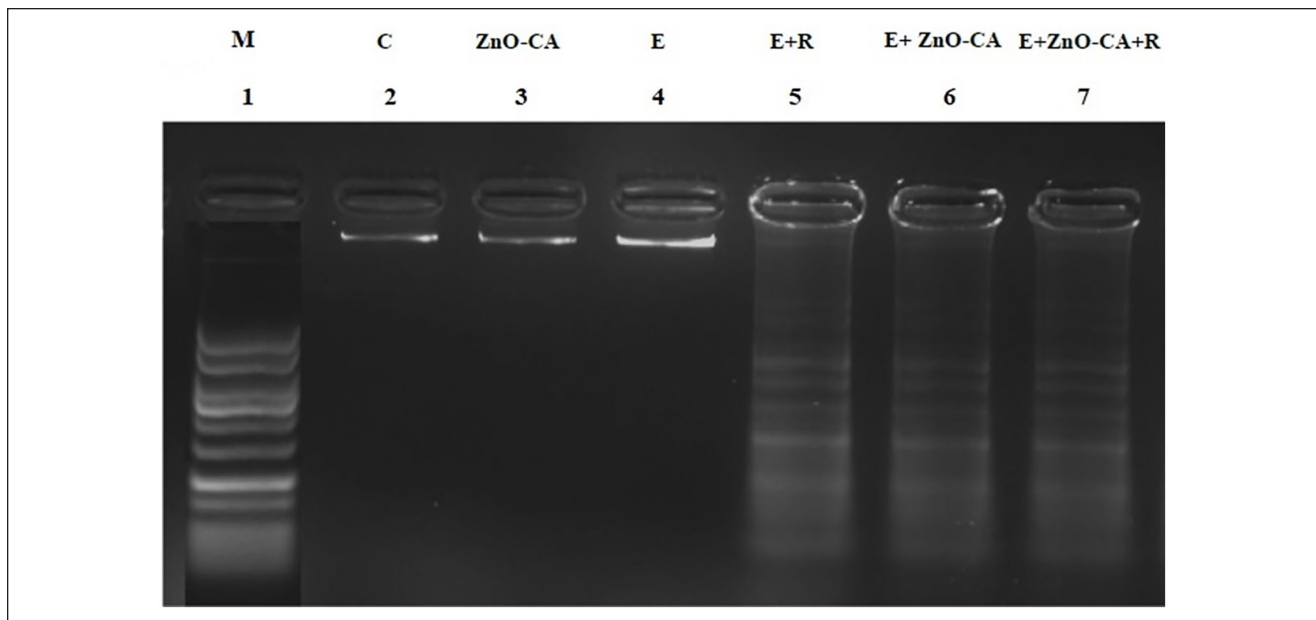
Figure (6). Effect of γ-Radiation Exposure and/or Zinc Oxide–Caffeic Acid Nanoparticles Treatment on the DNA fragmentation pattern. DNA marker (M) with 100-1000 base pair. C: control, E: Solid Ehrlich (EC) bearing mice, R: mice exposed to 2 Gy of whole-body gamma (γ)-irradiation/week for 3 consecutive weeks, and ZnO-CA: Mice injected intraperitoneally with 5 mg of Zinc Oxide–Caffeic acid nanoparticles (ZnO-CA NPs)/100 g body weight, every other day for 3 consecutive weeks. DNA fragmentation pattern was measured in thigh muscle of non-EC bearing mice (C and ZnO-CA NPs groups) or tumor tissues of solid EC bearing mice of different treated groups.

Table 4. Effect of γ-Radiation Exposure and/or Zinc Oxide–Caffeic Acid Nanoparticles Treatment on the Cell Cycle Modification.

Groups	SubG1	G0/G1	S phase	G2/M
C				
Mean ± SE	3.33 ± 0.24^a	85.07 ± 1.6^a	8.6 ± 0.84^{ac}	3.0 ± 0.67^{ae}
ZnO-CA				
Mean ± SE	2.97 ± 0.29^a	87.4 ± 0.6^a	7.9 ± 0.31^a	2.07 ± 0.52^a
%Change	−10.8	2.74	−8.14	−31
E				
Mean ± SE	3.1 ± 0.17^a	51.7 ± 1.71^b	26.5 ± 0.67^b	18.77 ± 0.55^b
%Change	−6.91	−39.23	208.14	525.67
E+R				
Mean ± SE	25.17 ± 0.38^b	49.17 ± 0.86^{bc}	9.87 ± 0.50^c	11.23 ± 0.28^c
%Change	655.86	−42.2	14.77	274.33
*%Change	711.94	−4.89	−62.75	−40.17
E+ZnO-CA				
Mean ± SE	22.23 ± 0.85^c	46.0 ± 0.83^c	8.87 ± 0.37^{ac}	10.0 ± 0.32^c
%Change	567.56	−45.93	−5.49	233.33
*%Change	617.1	−11.03	−67.66	−46.72
E+ZnO-CA+R				
Mean ± SE	39.9 ± 0.83^d	41.63 ± 0.67^d	4.91 ± 0.51^d	3.66 ± 0.15^e
% Change	1098	−51.06	−42.91	22
*% Change	1187.1	−19.47	−81.47	−80.5
F-ratio	827	333.69	184.85	204.53

Results are mean ± SE of 3 mice. Values with dissimilar superscripts are significantly different. % Change versus control group (C). * %Change versus untreated solid Ehrlich cancer (EC) bearing mice. C: control, E: Solid EC bearing mice, R: mice exposed to 2 Gy of whole body γ-irradiation/week, for 3 consecutive weeks, and ZnO-CA: mice injected intraperitoneally with 5 mg/100 g body weight ZnO-CA NPs, every other day for 3 consecutive weeks. Flow cytometry analysis of cell cycling was performed in the thigh muscle of non Ehrlich bearing mice (C and ZnO-CA groups) or tumor tissues of solid Ehrlich bearing mice of different treated groups. *P*-value < 0.001.
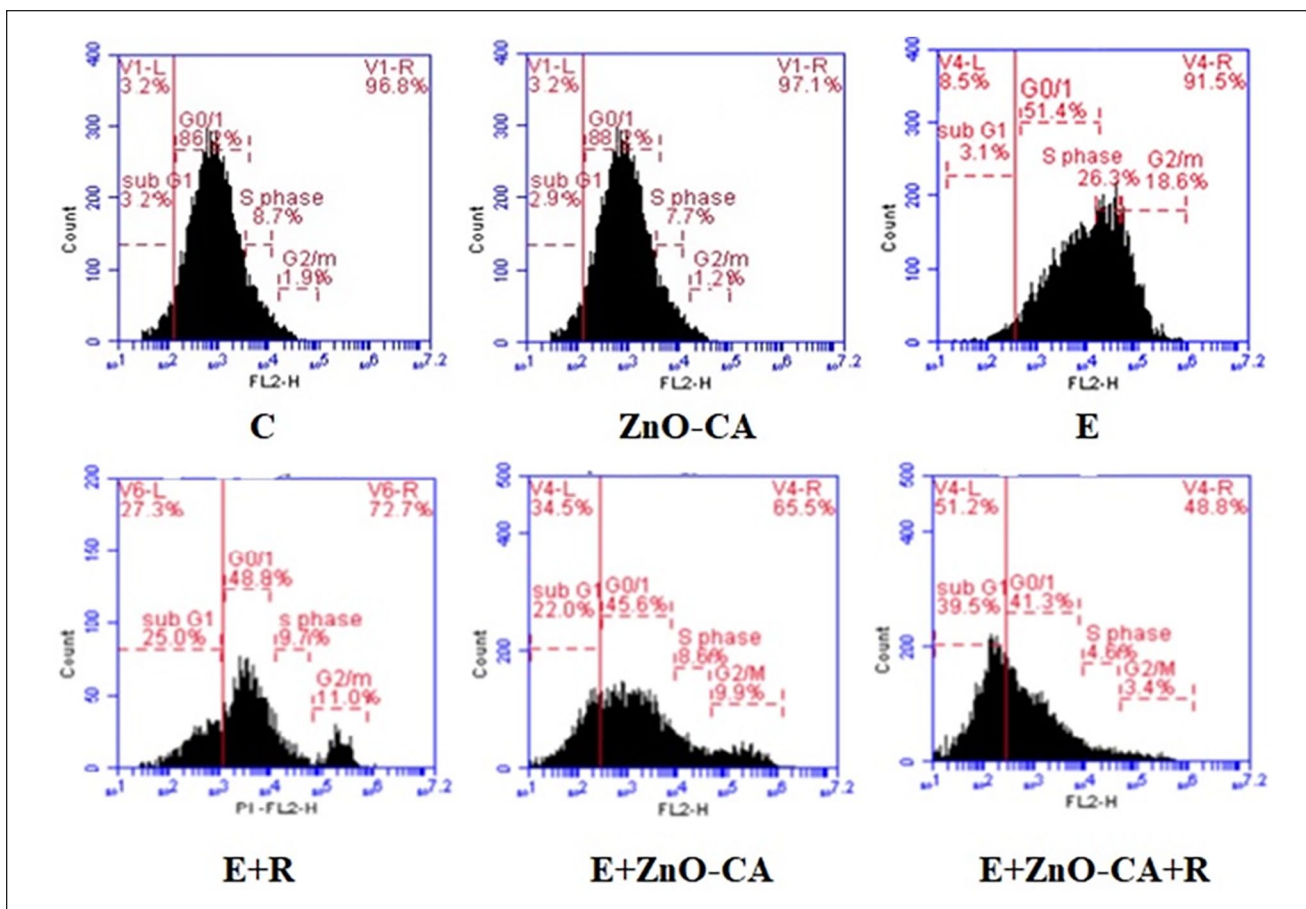
Figure 7. Flow cytometry analysis of cell cycling.
C: control, E: Solid Ehrlich (EC) bearing mice, R: mice exposed to 2 Gy of whole-body gamma (γ)-irradiation/week for 3 consecutive weeks, and ZnO-CA: Mice injected intraperitoneally with 5 mg of Zinc Oxide–Caffeic acid nanoparticles (ZnO-CA NPs)/100 g body weight, every other day for 3 consecutive weeks. Flow cytometry analysis of cell cycling was performed in thigh muscle of non-EC bearing mice (Control and ZnO-CA groups) or tumor tissues of solid EC bearing mice of different treated groups. P-value < 0.001.

COOH (acid), 1645 cm^{-1} is appointed to –C=O stretching vibration of –O–C=O, 1526 and 1451 cm^{-1} are appointed to C=C stretching vibration of phenol ring, 1354 and 1218 cm^{-1} are appointed to –O–H in-plane bending vibration of phenolic OH, 972 cm^{-1} is appointed to =C–H out-plane bending vibration of Ar–C=C, 851 cm^{-1} is appointed to out-plane bending vibration of CH in the aromatic ring with 2 neighboring hydrogen atoms, 816 cm^{-1} is appointed to in-plane bending vibration of C=O, 698 cm^{-1} is appointed to out-plane bending vibration of C=O.[50-52]

FT-IR spectra of ZnO NPs demonstrated that the distinguished bands detected around 471 and 521 cm^{-1} resulted from the stretching vibration of Zn-O bond in tetrahedral coordination. The band at 675 cm^{-1} is a very weak band formed due to the stretching vibrations of Zn-O bonds in octahedral arrangements. The band at 829 cm^{-1} is because of the configuration of tetrahedral coordinated Zn. The bands at 1558, 1507, and 1338 cm^{-1} can be correlated with the carboxylic group's symmetric

and asymmetric stretching vibrations resulting from the by-products or zinc acetate residues, remained after ZnO NPs fabrication.[53] The broad peak at 3393 cm^{-1} and the narrow one nearby 2876 cm^{-1} are because of O-H group and CO_2 stretching fashion,[54,55] which were presented due to the adsorption of moisture when FT-IR sample disc was prepared in an open atmosphere.[56] Consequently, FT-IR spectral analysis confirms the wurtzite structure of the prepared nanoparticles.[57,58] This outcome is complies with the results of former research.[56,59-61]

The successful amendment of ZnO NPs by CA was implemented by FT-IR spectroscopy. The signals: 829 cm^{-1}, 675 ν (Zn-O), 521 and 471 cm^{-1} confirm the ZnO NPs wurtzite structure. 1558, 1507, and 1338 cm^{-1} bands can be associated with the carboxylic group's symmetric and asymmetric stretching vibrations resulting from the by-products or zinc acetate residues, remained after ZnO NPs fabrication.[54] The broad signals at 3393 and 3314 cm^{-1} originate from the hydroxy group which belongs to both
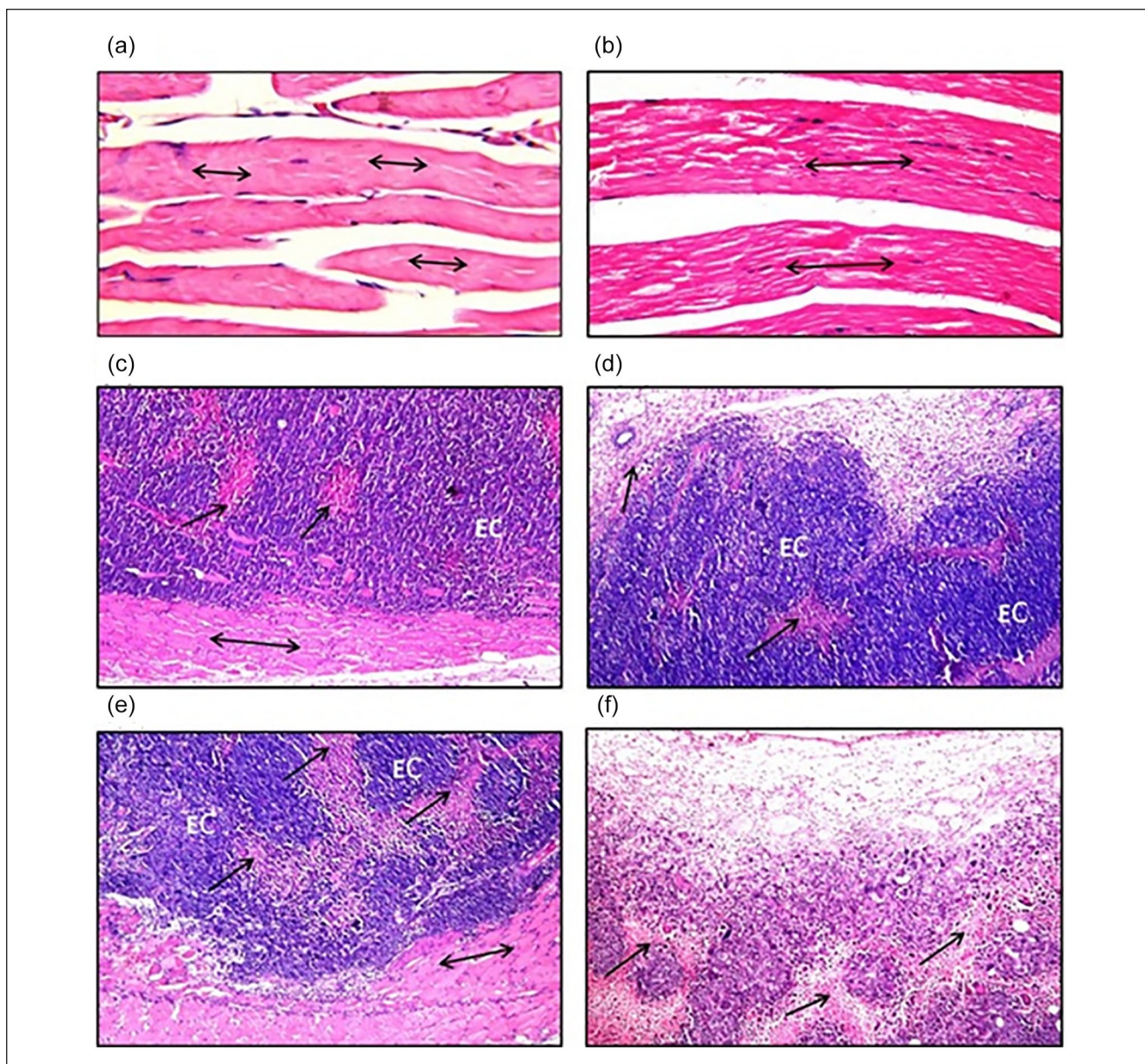
Figure 8. Histopathological photomicrographs of (a); thigh muscle of control mice (H&E stain, ×40), (b); thigh muscle of Zinc Oxide–Caffeic Acid nanoparticles (ZnO-CA NPs) treated mice (H&E stain, ×40), (c); solid Ehrlich carcinoma (EC) tumors of untreated mice, (d); solid Ehrlich carcinoma (EC) tumors of mice treated with gamma-irradiation (H&E stain, ×16), (e); solid Ehrlich carcinoma (EC) tumors of mice treated with Zinc Oxide–Caffeic acid nanoparticles (ZnO-CA NPs) (H&E stain, ×16), (f); solid Ehrlich carcinoma (EC) tumors of mice treated with gamma-irradiation and Zinc Oxide–Caffeic acid nanoparticles (ZnO-CA NPs) (H&E stain, ×16). Solid Ehrlich carcinoma (EC) tumor cells implanted between skeletal muscle bundles ($\leftrightarrow$) and criteria of malignancy necrosis ($\uparrow$).

samples (ZnO NPs and CA). Signals at 3057, 3026 and 2988 cm^{-1} are allocated to the C-H stretching vibration of phenol ring, the C-OH stretching vibrations band is shifted to 1269 cm^{-1} (instead of 1279 cm^{-1} in CA), 851 cm^{-1} is given to out-plane bending vibration of CH in the aromatic ring of CA. However, the weak signal at 1218 cm^{-1} in-plane bending modes of the CH-C=C, 1121 cm^{-1} in-plane bending modes of CH, weak signal at 972 cm^{-1} is assigned to =C–H out-plane bending vibration of Ar–C=C, the absence of

signals at 3431 and 3350 cm^{-1} ν(OH)arom, 2837–2565 cm^{-1} ν(OH)acid), 1645 cm^{-1} ν(C=O) and 1354 cm^{-1} ν(CC) + β(OH)) suggest that these molecules were adsorbed by the diph[29] relating the absence of those peaks to the adsorption of CA onto the surface of the ZnO NPs, and confirming the static interaction of CA and ZnO NPs.

A gradual decline in the viability percent and gradual increase in the toxicity percent of MCF7 and HepG2 cancer cells treated with different ZnO NPs concentrations was

perceived in a dose-dependent approach. This outcome follows the former results, where ZnO NPs demonstrated cytotoxicity on numerous cancer cell lines, including HepG2 human hepatocellular adenocarcinoma,[22] CAL 27 oral cancer,[62] and C2C12 mouse myoblast cell lines.[63] Besides, CA revealed cytotoxic activity against MCF7 and HepG2 cancer cell lines in the current study, which corroborates previous investigations using cervical,[64] fibrosarcoma[65] and colon cancer[66] cell lines. More interestingly, a synergistic cytotoxic effect for ZnO-CA NPs against HepG2 cells was recorded, which could reveal the capacity of CA to potentiate the cytotoxicity of ZnO NPs against cancer cells. Inconsistent with our finding, Balakrishnan et al[67] reported that gold nanoparticle–conjugated quercetin enhanced the anti-cancer effect of free quercetin, and increased apoptosis in breast cancer cells (MCF-7 and MDA-MB-231) more than free quercetin. The data also showed that ZnO-CA NPs exhibited in vivo anticancer activity against solid EC-bearing mice. The data also proved that ZnO-CA NPs and γ-irradiation act synergistically in reducing the volume and weight of solid tumors, which is in agreement with Abdallah et al[12] and Huang et al[68] who reported that combination treatment of nanoparticles and γ-radiation significantly suppressed tumor volume and weight in mice bearing tumors. Furthermore, the combined therapy showed a diminution of the tumor area with increasing necrotic cancer cells in the histopathological investigations, compared to ZnO-CA NPs or γ-irradiated single treatments.

In the present study, all mice bearing solid Ehrlich's carcinoma had a considerable increase in AST and ALT activities compared to untreated control, demonstrating the damage of hepatic tissues and release of transaminases into the blood stream.[69] It is well known that many functions of vital organs in the body may be impaired by the presence of tumor in the human body or experimental animals, even though the location of the tumor does not specifically interfere with this role. However, solid EC-bearing mice exposed to γ-irradiation displayed a considerable decrease in serum AST and ALT activities, compared to solid EC-bearing mice. This result is in agreement with (Abdelhalim and Moussa, 2013),[69] who mentioned that the values of those transaminases were considerably decreased with exposure of rats to different γ-irradiation doses. In this study, a more pronounced considerable decrease was observed in serum AST and ALT activities of solid EC-bearing mice treated with ZnO-CA NPs, only or combined with γ-irradiation, relative to solid untreated EC-bearing mice (E group). These findings may sustain the hepatoprotective activity of ZnO-CA NPs, especially when combined with gamma-radiation. It was demonstrated that CA maintains the structural integrity of the membranes against alcohol-intoxication,[70] and protects the liver from cadmium toxicity in rats,[71] which is in line with previous findings demonstrated that chitosan-coated nano-propolis protects liver and kidney against

cisplatin toxicity in rats, and that nano-propolis was more effective than propolis and had the potential to ameliorate cisplatin negative effects, while overcoming serious side effects such as liver and kidney damage.[72] The solid EC-bearing mice exposed to γ-irradiation displayed a slight considerable rise of serum urea level, while treatment of solid EC-bearing mice with ZnO-CA NPs, alone or combined with γ-radiation, exhibited a considerable increase in serum urea level compared to untreated solid EC-bearing mice. The increased serum urea could be attributed to enhanced protein breakdown after exposure to ionizing radiation, where the end product of protein catabolism is urea.[73]

The current study indicates that normal animals treated with ZnO-CA NPs manifest slight alterations in blood Hb concentration and PLTs count; several researchers reported similar results in animals treated with ZnO NPs.[74,75] This work demonstrated that mice bearing solid EC tumors manifest leukocytosis and thrombocytosis. It has been reported that the increase in WBCs and PLTs counts are associated with many tumor types.[76,77] Solid EC-bearing mice treated with γ-irradiation manifested a non-considerable decline in Hb concentration and a considerable decline in RBCs, WBCs, and PLTs counts, relative to untreated solid EC-bearing mice. Younis et al[78] demonstrated that RT can cause a decrease in the number of RBCs and Hb concentration in cancer patients. The peroxide formation and membrane cross-linkages by γ-irradiation may disturb the lipid bilayer upper region by inducing water diffusion and ultimately causing hemolysis of RBCs.[79] Mice bearing solid-EC treated with ZnO-CA NPs and/or γ-irradiation recorded a sharp considerable decrease in WBCs, and PLTs counts, compared to untreated EC-bearing mice. It is well known that CT and RT significantly lower WBCs and PLTs counts in patients.[80]

The mitogen-activated protein kinase (MAPK) is one such complex interconnected signaling cascade with frequent involvement in oncogenesis, tumor progression, and drug resistance. The MAPK family consists of a large number of kinases that altered in cancers. The upregulation of the MAPK signaling pathway, including p38 MAPK, JNK, and ERK1/2 can activate transcription factors such as NF-κB.[81] NF-κB activates the transcription of several genes involved in the suppression of cell death by the mitochondrial pathway, whereas the anti-apoptotic members of the Bcl-2 family antagonize the function of the pro-apoptotic members. NF-κB also induces the expression of cell adhesion molecules including E-selectin, intracellular adhesion molecule-1 (ICAM-1), and VCAM-1. The expression of genes involved in many processes that play a key role in the development and progression of cancer such as proliferation, migration, and apoptosis are regulated by NF-kB.[82]

The results demonstrate that inoculation of solid EC tumors into female mice caused considerable upregulation

in BCL2 and NF-κB gene expression, and enhancement in VCAM-1 level, along with a significant upregulation of p-ERK1/2 protein expression in the tumor tissue, compared to control animals. Campbell and Tait[83] mentioned that deregulation of Bcl2 proteins is now known as a common occurrence in numerous cancer categories, and it is probable that pro-survival Bcl2 proteins regulation will bring about an improvement to the existing tumor therapeutic approaches. Additionally, DiDonato et al[84] reported that NF-κB regulates the expression of genes that influence the growth and progression of cancer. In several human malignancies, constitutive or aberrant NF-κB activation was previously reported.[85] Furthermore, ERK1/2 signaling is involved as a main cell proliferation organizer, and for this purpose, the ERK pathway inhibitors are entering clinical studies as promising anticancer agents.[86] The development of numerous immunological disorders, including transplant rejection, asthma, rheumatoid arthritis, and cancer, are closely associated with VCAM-1.[87] VCAM-1 may be accompanied by tumor progression and metastasis.[88]

In this work, exposure of solid EC-bearing mice to γ-irradiation produced a marked downregulation in BCL2 and NF-κB gene expression and a considerable decline in VCAM-1 level as well as a remarkable downregulation in p-ERK1/2 protein expression in the tumor tissue, compared to untreated EC-bearing mice. Filippovich et al[89] reported that irradiation directed the human myeloma cell line to apoptosis via Bcl-2, and caspase-3 cleavage, leading to DNA degradation. Also, Wunderlich et al[90] observed a considerable decrease in NF-κB, p65, and IL-1β by applying a single dose of 0.5 up to 2.0 Gy, in pre-activated peritoneal macrophages of the radiosensitive BALB/c mice.

Comparable results were detected in solid EC-bearing mice treated with ZnO-CA NPs. The mitochondrial apoptotic pathway also mediates the genotoxic and cytotoxic potential of ZnO NPs, whereas ROS reduced the mitochondrial membrane potential and enhanced the Bax/Bcl2 ratio.[91] Kim and Jeong[92] reported that ZnO NPs blocked IκBα phosphorylation and degradation, and accordingly inhibited the nuclear translocation of NF-κB in RAW 264.7 macrophages. Also, Kim et al[93] mentioned that CA inhibits the NF-κB activation in endothelial cells via the c-Src/ERK and NIK/IKK signal transduction pathways. Min et al[94] and Chang et al[64] reported that CA provoked apoptosis via inhibiting Bcl-2, the liberation of cytochrome c, and caspase-3 activation, suggesting that CA prompted apoptosis via the mitochondrial apoptotic pathway, which implies strong anti-tumor chemopreventive or chemotherapeutic activities of CA. On the contrary, Sun et al[95] reported that ZnO NPs significantly increased the mRNA levels of the inflammatory markers VCAM-1, ICAM-1, MCP-1, and IL-8 in human cardiac microvascular endothelial cells, suggesting the protective effect of CA against the inflammatory response induced by ZnO NPs, which is in line with the previous finding that CA inhibits VCAM-1 expression in human umbilical vein endothelial cells.[96]

Combined treatment of ZnO-CA NPs and γ-irradiation demonstrated a synergistic potential in down-regulating tumor BCL2 and NF-κB gene expression, decreasing VCAM-1 level and down-regulating p-ERK1/2 protein expression in tumor tissues, compared to EC-bearing mice. This result is in agreement with Abdallah et al[12] who reported that combined treatment of EC-bearing mice with gadolinium oxide nanocomposite and radiation led to a highly significant decrease in mitochondrial enzymes' activities, with activation of caspase-3 and a significant increase in DNA fragmentation. Additionally, Nan et al[97] mentioned that quercetin-loaded chitosan nanoparticles notably enhance the effect of quercetin, one of the flavonoid family members, on inhibiting the NF-κB/COX-2 signaling pathway as well as ameliorating the skin edema caused by UVB radiation. Furthermore, Wu et al[98] observed downregulation of ICAM-1 in cells treated with gold NPs, causing a strong inhibition of cell invasion potential.

Although RT-induced toxicity to cancer cells starts promptly and continues for weeks to months after the end of treatment, cancer cell resistance to ionizing radiation (IR) frequently causes local recurrences and metastases.[99,100] Thus, understanding the molecular mechanisms responsible for radioresistance is crucial to improving RT treatment. IR destroys cancer cells by inducing DNA damage, either directly or indirectly, through highly reactive oxygen species (ROS)-mediated DNA damage. DNA damage includes DNA double-strand breaks (DSBs), the most lethal form of damage, which in turn leads to apoptosis-, necrosis-, and senescence- or autophagy-mediated cancer cell death.[101] Furthermore, IR promotes cancer cell death by activating the host anti-tumor immunity.[102]

Cancer cells may evade IR-induced cell death through different mechanisms.[101] Indeed, the success of RT is determined by the ability of treatment (i) to induce irreparable DNA damages; (ii) to redistribute the surviving cells into the G2/M cell cycle phase, which is the most radiosensitive phase; (iii) to prevent the surviving cells from repopulating the death fraction, and (iv) to promote the re-oxygenation of hypoxic tumor areas.[102] Following radiation, ERK1/2 is activated, which sustains cancer cell radioresistance, through dual tyrosine and threonine phosphorylation by the mitogen-activated protein kinase kinase enzyme (MEK1/2), and the activation, in turn, leads to the phosphorylation/activation of over 160 substrates.[103] Collectively, inhibition of ERK1/2 activation and reduction in checkpoint activation increases sensitivity of cells to DNA damage, which may cause apoptosis, thereby enhancing chemotherapy's efficacy.[104,105]

Exposure of solid EC-bearing mice to γ-irradiation and/or treatment with ZnO-CA NPs induced DNA damage, as

evidenced by the appearance of DNA strand breaks. DNA has commonly been known to be the critical target for ionizing radiation-induced cell death. Ionizing radiations causes the formation of more complex lesions, and multiply damaged sites within the DNA helical turns, breaking the double- and single strands, thus triggering DNA base damage that results in mutations and cell death.[106] ZnO NPs induced cytotoxicity and oxidative DNA breakdown in numerous tumor cell lines[91,107] due to the intracellular ROS and oxidative stress assembly. Abdallah et al[12] mentioned that treatment of EC-bearing mice with gadolinium oxide nanocomposite and γ irradiation produced a remarkable inhibition of DNA repair and inhibition of DNA synthesis. Additionally, Subiel et al[108] showed that metal-based nano-enhancers could increase the number of initial double-strand breaks (DSBs) in DNA following irradiation.

Numerous studies mentioned that ZnO-NPs treatment resulted in a deposition and recognizable peak at sub-G_0/G_1 that indicates the apoptotic and dead cell population.[109-112] Additionally, Murad et al[113] reported that ionizing radiation decreased cell viability of human glioblastoma T98G cell line, and considerably enhanced the sub G_0/G_1 phase. Several investigations reported that CA or its related compound caffeic acid phenyl ester (CAPE) successfully repressed the cancer cells propagation in vitro, through the activation of cell cycle arrest at the G_0/G_1 phase, in different cell lines.[66,94,114] In agreement with the previous finding, a significant increase in the sub G1 population in the tumor tissue of solid EC-bearing mice treated with ZnO-CA NPs was recorded, either alone or combined with γ-irradiation, associated with a considerable decline in G_0/G_1 as well as S phase and G2/M populations denoting a remarkable increase in the dead cell population and cell cycle arrest at G_0/G_1, compared to untreated EC-bearing mice. Inconsistent with this, Abdallah et al[12] reported the synergistic effect of gadolinium oxide nanocomposite and radiation for induction of cell cycle arrest and apoptosis.

Solid EC mice exposed to radiation alone did not acquire show resistance to γ radiation, and this evidence may be due to ERK1/2 inhibition, unrepaired DNA damage, and decline in G2/M population; however, ZnO-CA NPs showed a strong ability to enhance the radiosensitivity of solid EC tumor compared to γ-irradiation alone.

Finally, this work demonstrates that ZnO-CA NPs radiosensitization mechanisms may consist of ROS generation, targeting of DNA damage response, and repair, oxidative stress, mitochondrial dysfunction, suppression of cell cycle checkpoint machinery, and promoting cell death by a variety of mechanisms such as apoptosis, and necrosis, accompanied by downregulation of p-ERK 1/2 protein expression, BCL2 and NF-κB gene expressions, as well as VCAM-1 level inhibition.

Animal experiments are frequently performed to provide scientific data and/or to elucidate the mechanisms before the clinical manipulation of the newly formulated drug. Dose conversion from animal to human is a critical step during developing a new drug. To choose a suitable starting dose for the initial clinical trials, the animal dose should be extrapolated to humans depending on the body surface area (BSA), not only on the body weight, as recommended by previous investigation.[37] Body surface area scaling has been used to determine human dosages for a variety of drugs, and FDA has recommended it as one method for using data from animal model species to determine a safe starting dose for human clinical trials.[115] It also provides a more conservative dose estimate, especially for nanomaterials.[116] Generally, the body surface area seems to have a good correlation among species with several parameters including oxygen utilization, caloric expenditure, basal metabolism, blood volume, and circulating plasma protein.[37,117] Valic and Zheng[116] mentioned that the clinical starting dose may be determined by dividing the estimated human equivalent dose (HED) of the rodent by a safety factor with a default value of 10. The safety factor allows variability in extrapolating from animal toxicity studies in humans resulting from uncertainties due to enhanced sensitivity to pharmacologic activity in humans versus animals, difficulties in detecting certain pathologies in animals (eg, headache, myalgia, and mental disturbances), differences in receptor densities or affinities, and unexpected toxicities.[117] ZnO NPs are considered as "generally recognized as safe" and are approved by FDA and the health risks of ZnO NPs and ZnO microparticles (ZnO MPs) are guided by the Organization for Economic Cooperation and Development, based on their unique physicochemical characteristics via synthesis techniques.[118] The risk assessments of ZnO NPs via different exposure routes are necessary to explore their clinical use. Accordingly, the use of ZnO NPs by humans should be carefully considered.[118] According to our results that reflect the potential anticancer activity of ZnO-CA NPs, CA may imply strong chemopreventive effects against any probable toxicity induced by ZnO NPs.

Conclusion

Zinc Oxide-Caffeic acid (ZnO-CA) NPs are prepared in a simple method and exhibit in vitro and in vivo anticancer activities. The in vivo ZnO-CA NPs anticancer activity is augmented upon exposure of animals to γ-irradiation. The obtained results indicate the effectiveness of ZnO-CA NPs in the treatment of EC-tumor, whereas γ-irradiation augents this effect. Further investigations on ZnO-CA NPs radiosensitization should be performed on an animal-model for a long period of time after irradiation treatment, or in a radioresistant cancer cell type. As well as, further explorations are warranted previous to the clinical application of ZnO-CA NPs.

Author Contributions

Hayam M. Sayed: Conceptualization, Methodology, Writing—original draft. Mahmoud M. Said: Data curation, formal analysis, Supervision, Writing—original draft. Nadia Y. S. Morcos: Supervision, Writing—original draft. Mona A. El Gawish: Supervision, Writing—original draft. Amel F. M. Ismail: Supervision, Methodology, Writing—original draft, review and editing.

ORCID iD

Amel F. M. Ismail [ID] https://orcid.org/0000-0002-3446-2372

References

1. Bray F, Ferlay J, Soerjomataram I, Siegel RL, Torre LA, Jemal A. Global cancer statistics GLOBOCAN estimates of incidence and mortality worldwide for 36 cancers in 185 countries. *CA Cancer J Clin*. 2018;68:394-424. doi:10.3322/caac.21492

2. Li L, Zhang W, Zhao S, Sun M. FOS-like antigen 1 is a prognostic biomarker in hepatocellular carcinoma. *Saudi J Gastroenterol*. 2019;25:369-376. doi:10.4103/sjg.SJG_595_18

3. Liu Y-Q, Wang X-L, He D-H, Cheng Y-X. Protection against chemotherapy- and radiotherapy-induced side effects: a review based on the mechanisms and therapeutic opportunities of phytochemicals. *Phytomedicine*. 2021;80:153402. doi:10.1016/j.phymed.2020.153402.

4. Efferth T, Saeed MEM, Kadioglu O, et al. Collateral sensitivity of natural products in drug-resistant cancer cells. *Biotechnol Adv*. 2020;38:107342. doi:10.1016/j.biotechadv.2019.01.009

5. Mbaveng AT, Bitchagnoc GTM, Kuetea V, Tane P, Efferth T. Cytotoxicity of ungeremine towards multi-factorial drug resistant cancer cells and induction of apoptosis, ferroptosis, necroptosis and autophagy. *Phytomedicine*. 2019;60:152832. doi:10.1016/j.phymed.2019.152832

6. Boulos JC, Rahama M, Hegazy MF, Effert T. Shikonin derivatives for cancer prevention and therapy. *Cancer Letters*. 2019;459:248-267. doi:10.1016/j.canlet.2019.04.033

7. Lorenz V, Liebing P, Suta M, et al. Synthesis, structure, complexation, and luminescence properties of the first metal-organic curcumin compound Bis (4-triphenylsiloxy) curcumin. *J Lumin*. 2019;211:243-250. doi:10.1016/j.jlumin.2019.02.058

8. Hou Q, He C, Lao K, Luo G, Xiang H. Design and synthesis of novel steroidal imidazoles as dual inhibitors of AR/CYP17 for the treatment of prostate cancer. *Steroids*. 2019;150:108384. doi:10.1016/j.steroids.2019.03.003

9. Cryer AM, Thorley AJ. Nanotechnology in the diagnosis and treatment of lung cancer. *Pharmacol Ther*. 2019;198:189-205. doi:10.1016/j.pharmthera.2019.02.010

10. Liu Y, Zhang P, Li F, et al. Metal based *NanoEnhancers* for future radiotherapy: radiosensitizing and synergistic effects on tumor cells. *Theranostics*. 2018;8:1824-1849. doi:10.7150/thno.22172

11. Raviraj J, Bokkasam VK, Kumar VS, Reddy US, Suman V. Radiosensitizers, radioprotectors, and radiation mitigators. *Ind J Dent Res*. 2014;25:83-90. doi:10.4103/0970-9290.131142

12. Abdallah NM, Noman E, Eltahawy NA, et al. Anticancer and radiosensitization efficacy of nanocomposite *Withania somnifera* extract in mice bearing tumor cells. *Asian Pac J Cancer Prev*. 2016;17:4367-4375.

13. Rasmussen JW, Martinez E, Louka P, Wingett DG. Zinc oxide nanoparticles for selective destruction of tumor cells and potential for drug delivery applications. *Expert Opin Drug Del*. 2010;7:1063-1077. doi:10.1517/17425247.2010.502560

14. Krishna PG, Ananthaswamy PP, Trivedi P, et al. Antitubercular activity of ZnO nanoparticles prepared by solution combustion synthesis using lemon juice as biofuel. *Mater Sci Eng C*. 2017;75:1026-1233. doi:10.1016/j.msec.2017.02.093

15. Dogra S, Kar AK, Girdhar K, et al. Zinc oxide nanoparticles attenuate hepatic steatosis development in high-fat-diet fed mice through activated AMPK signaling axis. *Nanomedicine*. 2019;17:210-222. doi:10.1016/j.nano.2019.01.013

16. Anan HH, Zidan RA, Abd EL-Baset SA, Ali MM. Ameliorative effect of zinc oxide nanoparticles on cyclophosphamide induced testicular injury in adult rat. *Tissue Cell*. 2018;54:80-93. doi:10.1016/j.tice.2018.08.006

17. De Berrardis B, Civitelli G, Condello M, et al. Exposure to ZnO nanoparticles induces oxidative stress and cytotoxicity in human colon carcinoma cells. *Toxicol Appl Pharm*. 2010;246:116-127. doi:10.1016/j.taap.2010.04.012

18. Layne JC. *Zinc oxide nanoparticles as potential novel anticancer therapies*. Boise State University Theses and Dissertations; 2011:194. https://scholarworks.boisestate.edu/td/194

19. Santhosh PB, Ulrih NP. Multifunctional superparamagnetic iron oxide nanoparticles: promising tools in cancer theranostics. *Cancer Lett*. 2013;336:8-17. doi:10.1016/j.canlet.2013.04.032

20. Stan M, Popa A, Toloman D, Silipas T-D, Vodnar DC. Antibacterial and antioxidant activities of ZnO nanoparticles synthesized using extracts of allium sativum, rosmarinus officinalis and ocimum basilicum. *Acta Metall Sin Engl Lett*. 2016;29:228-236. doi:10.1007/s40195-016-0380-7

21. Anitha R, Ramesh KV, Ravishankar TN, Kumar KHS, Ramakrishnappa T. Cytotoxicity, antibacterial and antifungal activities of ZnO nanoparticles prepared by the Artocarpus gomezianus fruit mediated facile green combustion method. *J Sci Adv Mat Dev*. 2018;3:440-451. doi:10.1016/j.jsamd.2018.11.001

22. Ismail AFM, Ali MM, Ismail LFM. Photodynamic therapy mediated antiproliferative activity of some metal-doped ZnO nanoparticles in human liver adenocarcinoma HepG2 cells under UV irradiation. *J Photochem Photobiol B*. 2014;138:99-108. doi:10.1016/j.jphotobiol.2014.04.006

23. Lee JM, Choi K-H, Min J, Kim H-J, Jee J-P, Park BJ. Functionalized ZnO nanoparticles with gallic acid for antioxidant and antibacterial activity against methicillin-resistant S. aureus. *Nanomaterials*. 2017;7:365. doi:10.3390/nano7110365

24. Fanga X, Jianga L, Gonga Y, Lia J, Liub L, Cao Y. The presence of oleate stabilized ZnO nanoparticles (NPs) and reduced the toxicity of aged NPs to Caco-2 and HepG2 cells. *Chem Biol Interact*. 2017;278:40-47. doi:10.1016/j.cbi.2017.10.002

25. Wang J, Lee JS, Kim D, Zhu L. Exploration of zinc oxide nanoparticles as a multitarget and multifunctional anticancer nanomedicine. *ACS App Mater Interfaces*. 2017;9:39971-39984. doi:10.1021/acsami.7b11219

26. Puvvada N, Rajput S, Kumar BN, et al. Novel ZnO hollow-nanocarriers containing paclitaxel targeting folate receptors in a malignant pH-microenvironment for effective monitoring and promoting breast tumor regression. *Sci Rep*. 2015;5:11760. doi:10.1038/srep11760

27. Zhang T, Wojtal P, Rubel O, Zhitomirsky I. Density functional theory and experimental studies of caffeic acid adsorption on zinc oxide and titanium dioxide nanoparticles. *RSC Adv*. 2015;5:106877-106885. doi:10.1039/C5RA21511K

28. Belay A, Kim HK, Hwang YH. Probing the interaction of caffeic acid with ZnO nanoparticles. *J Lumin*. 2016;31:654-659. doi:10.1002/bio.3007

29. Choi K-H, Nam K C, Lee S-Y, Cho G. Antioxidant potential and antibacterial efficiency of caffeic acid-functionalized ZnO nanoparticles. *Nanomaterials*. 2017;7:148. doi:10.3390/nano7060148

30. Belay A, Kim HK, Hwang YH. Binding of caffeine with caffeic acid and chlorogenic acid using fluorescence quenching. *J Lumin*. 2016;31:565-572. doi:10.1002/bio.2996

31. Espindola KMM, Ferreira RG, Narvaez LEM, et al. Chemical and pharmacological aspects of caffeic acid and its activity in hepatocarcinoma. *Front Oncol*. 2019;9:541. doi:10.3389/fonc.2019.00541

32. Almeida AA, Farah A, Silva DAM, Nunam EA, Glória MBA. Antibacterial activity of coffee extracts and selected coffee chemical compounds against enterobacteria. *J Agric Food Chem*. 2006;54:8738-8743. doi:10.1021/jf0617317

33. Orsolic NL, Sver S, Terzi´ CL, Basi´ C. Peroral application of water-soluble derivative of propolis (WSDP) and its related polyphenolic compounds and their influence on immunological and antitumour activity. *Vet Res Commun*. 2005;29:575-793. doi:10.1007/s11259-005-3303-z

34. Saif M, Hafez H, Nabeel AI. Photo-induced self-cleaning and sterilizing activity of Sm^3+doped ZnO nanomaterials. *Chemosphere*. 2013;90:840-847.doi:10.1016/j.chemosphere.2012.09.095

35. Hariharan R, Senthilkumara S, Suganthib A, Rajarajan M. Synthesis and characterization of daunorubicin modified ZnO/PVP nanorods and its photodynamic action. *J Photochem Photobiol A*. 2013;252:107-115. doi:10.1016/j.jphotochem.2012.11.017

36. Akhila JS, Deepa S, Alwar MC. Acute toxicity studies and determination of median lethal dose. *J Curr Sci*. 2007;93:917-20.

37. Nair AB, Jacob S. A simple practice guide for dose conversion between animals and human. *J Basic Clin Pharma*. 2016;7:27-31. doi:10.4103/0976-0105.177703

38. Plumb JA. Cell sensitivity assays: clonogenic assay. In: SP, Langdon ed. *Methods in Molecular Medicine*. Humana Press; 2004:88:159-164. doi:10.1385/1-59259-406-9:159

39. El-Bahy AA, Abou-Aisha K, Noaman E, Mahran LG. Regression of murine Ehrlich ascites carcinoma using tumor-targeting Salmonella VNP20009-comparison with the effect of the anticancer drug doxorubicin. *Adv Cancer Res Treat*. 2012;2012:125978. doi: 10.5171/2012.125978

40. Jensen MM, Jorgensen JT, Binderup T, Kjaer A. Tumour volume in subcutaneous mouse xenografts measured by micro CT is more is more accurate and reproducible than determined by F-FDG-micro PET or external caliper. *J BMC Med Imaging*. 2008;8:16. doi:10.1186/1471-2342-8-16

41. Xu W, Guo G, Li J, et al. Activation of Bcl-2-Caspase-9 apoptosis pathway in the testis of asthmatic mice. *PLoS One*. 2016;11:e0149353. doi:10.1371/journal.pone.0149353

42. Yamamoto H, Omelchenko I, Shi X, Nuttall AL. The influence of NF-κB signal-transduction pathways on the murine inner ear by acoustic overstimulation. *J Neurosci Res*. 2009;87:1832-1840. doi:10.1002/jnr.22018

43. Livak KJ, Schmittgen TD. Analysis of relative gene expression data using real time quantitative PCR and the2⁻ΔΔCt method. *Methods*. 2001;25:402-408. doi:10.1006/meth.2001.1262

44. Okamura K, Hagiwara-Takeuchi Y, et al. Comparative genome analysis of the mouse imprinted gene Impact and its nonimprinted human homolog IMPACT: toward the structural basis for species-specific imprinting. *Genome Res*. 2000;10:1878-1889. doi:10.1101/gr.139200

45. Givan AL. *Flow Cytometry: First Principles*. 2nd ed. Wiley, John & Sons, Inc; 2001. doi:10.1002/0471223948

46. Bancroft JD, Steven A, Turner DR. *Theory and Practice of Histological Techniques*. 4th edn. Churchill Livingston; 2013. doi:10.1111/j.1365-2559.1990.tb00755.x

47. Gu F, Wang SF, Lu MK, Zhou GJ, Xu D, Yuan DR. Structure evaluation and highly enhanced luminescence of Dy3+-doped ZnO nanocrystals by Li+ doping via combustion. *Method Langmuir*. 2004;20:3528-3531. doi:10.1021/la049874f

48. Naga Raju B, Siva Kumar S, Prasad VSRK, Ramji K. Synthesis and characterization of high pure ZnO nano particles by conventional methods, *Int J Nanotechnol Appl*. 2010;3:199-205.

49. Barick K, Sarika Singh C, Aslam M, Bahadur D. Porosity and photocatalytic studies of transition metal doped ZnO nanoclusters. *Microporous Mesoporous Mater*. 2010;134:195-202. doi:10.1016/j.micromeso.2010.05.026

50. Świsłocka R. Spectroscopic (FT-IR, FT-Raman, UV absorption, 1H and 13C NMR) and theoretical (in B3LYP/6-311++G** level) studies on alkali metal salts of caffeic acid. *Spectrochim Acta A*. 2013;100:21-30. doi:10.1016/j.saa.2012.01.048

51. Kumar N, Pruthi V, Goel N. Structural, thermal and quantum chemical studies of *p*-coumaric and caffeic acids. *J Mol Struct*. 2015;1085:242-248. doi:10.1016/j.molstruc.2014.12.064

52. Xing Y, Peng HY, Zhang MX, Li X, Zeng WW, Yang XE. Caffeic acid product from the highly copper-tolerant plant Elsholtzia splendens post-phytoremediation: its extraction, purification, and identification. *J Zhejiang Univ Sci B*. 2012;13:487-493. doi:10.1631/jzus.B1100298

53. Noah AZ, El Semary MA, Youssef AM, El-Safty MA. Enhancement of yield point at high pressure high temperature wells by using polymer nanocomposites based on ZnO & CaCO₃ nanoparticles. *Egypt J Pet*. 2017;26:33-40. doi:10.1016/j.ejpe.2016.03.002

54. Udayakumar S, Renuka V, Kavitha K. Structural, optical and thermal studies of cobaltdoped hexagonal ZnO by simple chemical precipitation method. *J Chem Pharm Res*. 2012;4:1271-1280.

55. Ravichandrika K, Kiranmayi P, Ravikumar RV. Synthesis, characterization and antibacterial activity of ZnO nanoparticles. *In J Pharm Pharm Sci*. 2012;4:336-338.

56. Meena RK, Chouhan N. ZnO nanoparticles synthesized by a novel approach at room temperature and antibacterial activity. *Science*. 2015;15:68-72.

57. Guo Y, Cao X, Lan X, Zhao C, Xue X, Song Y. Solution-based doping of manganese into colloidal ZnO nanorods. *J Phys Chem C*. 2008;112:8832-8838. doi:10.1021/jp800106v

58. Kumar S, Mukherjee S, Singh R, Kr Chatterjee S, Ghosh AK. Structural and optical properties of sol-gel derived nanocrystalline Fe-doped ZnO. *J Appl Phys*. 2011;110:103508. doi:10.1063/1.3658221

59. Hedayati K. Fabrication and optical characterization of zinc oxide nanoparticles prepared via a simple sol-gel method. *J Nanostructures*. 2015;5:395-401. doi:10.7508/JNS.2015.04.010

60. Ntwaeaborwa OM, Mofokeng SJ, Kumar V, Kroon RE. Structural, optical and photoluminescence properties of Eu3+ doped ZnO nanoparticles. *Spectrochim Acta A Mol Biomol Spectrosc*. 2017;182:42-49. doi:10.1016/j.saa.2017.03.067

61. Sharma D, Jha R. Transition metal (Co, Mn) co-doped ZnO nanoparticles: effect on structural and optical properties. *J Alloys and compd*. 2017;698:532-538. doi:10.1016/j.jallcom.2016.12.227

62. Wang J, Gao S, Wang S, Xu Z, Wei L. Zinc oxide nanoparticles induce toxicity in CAL 27 oral cancer cell lines by activating PINK1/Parkin-mediated mitophagy. *Int J Nanomed*. 2018;13:3441-3450. doi:10.2147/IJN.S165699

63. Pandurangan M, Kim DH. ZnO nanoparticles augment ALT, AST, ALP and LDH expressions in C2C12 cells. *Saudi J Biol Sci*. 2015;22:679-684. doi:10.1016/j.sjbs.2015.03.013

64. Chang WC, Hsieh CH, Hsiao MW, Lin WC, Hung YC, Ye JC. Caffeic acid induces apoptosis in human cervical cancer cells through the mitochondrial pathway. *Taiwan J Obstet Gynecol*. 2010;49:419-424. doi:10.1016/S1028-4559(10)60092-7

65. Rajendra Prasad N, Karthikeyan A, Karthikeyan S, Reddy BV. Inhibitory effect of caffeic acid on cancer cell proliferation by oxidative mechanism in human HT-1080 fibrosarcoma cell line. *Mol Cell Biochem*. 2011;349:11-19. doi:10.1007/s11010-010-0655-7

66. Chiang EP, Tsai SY, Kuo YH, et al. Caffeic acid derivatives inhibit the growth of colon cancer: involvement of the PI3-K/Akt and AMPK signaling pathways. *PLoS One*. 2014;9:e99631. doi:10.1371/journal.pone.0099631

67. Balakrishnan S, Bhat FA, Raja Singh P, et al. Gold nanoparticle-conjugated quercetin inhibits epithelial-mesenchymal transition, angiogenesis and invasiveness via EGFR/VEGFR-2-mediated pathway in breast cancer. *Cell Prolif*. 2016;49:678-697. doi:10.1111/cpr.12296

68. Huang C, Chen T, Zhu D, Huang Q. Enhanced tumor targeting and radiotherapy by quercetin loaded biomimetic nanoparticles. *Front Chem*. 2020;8:225. doi:10.3389/fchem.2020.00225

69. Abdelhalim MAK, Moussa SAA. The biochemical changes in rats' blood serum levels exposed to different γ-irradiation doses. *Afr J Pharm Pharmacol*. 2013;7:785-792. doi:10.5897/AJPP2013.3434

70. Pari L, KarthiKesan K. Protective role of caffeic acid against alcohol-induced biochemical changes in rats. *Fundam Clin Pharmacol*. 2007;21:355-361. doi:10.1111/j.1472-8206.2007.00505.x

71. Ashour TH. Preventative effects of caffeic acid phenyl ester on cadmium intoxication induced hematological and blood coagulation disturbances and hepatorenal damage in rats. *ISRN Hematol*. 2014;2014:764754,7. doi:10.1155/2014/764754

72. Tatli Seven P, Seven I, Karakus S, et al. Turkish propolis and its nano form can ameliorate the side effects of cisplatin, which is a widely used drug in the treatment of cancer. *Plants*. 2020;9:1075. doi:10.3390/plants9091075

73. Moulder JE, Fish BL, Regner KR, Cohen EP, Raife TJ. Retinoic acid exacerbates experimental radiation nephropathy. *Radiat Res*. 2002;157:199-203. doi:10.1667/0033-7587(2002)157[0199:RAEERN]2.0.CO;2

74. Yan G, Huang Y, Bu Q, et al. Zinc oxide nanoparticles cause nephrotoxicity and kidney metabolism alterations in rats. *J Environ Sci Health A Tox Hazard Subst Environ Eng*. 2012;47:577-588. doi:10.1080/10934529.2012.650576

75. Ko J-W, Hong E-T, Lee I-C, et al. Evaluation of 2-week repeated oral dose toxicity of 100 nm zinc oxide nanoparticles in rats. *Lab Anim Res*. 2015;31(3):139-147. doi:10.5625/lar.2015.31.3.139

76. Carr BI, Guerra V. Thrombocytosis and hepatocellular carcinoma. *Dig Dis Sci*. 2013;58:1790-1796. doi:10.1007/s10620-012-2527-3

77. Mantas D, Kostakis ID, Machairas N, Markopoulos C. White blood cells and platelet indices as prognostic markers in patients with invasive ductal breast carcinoma. *Oncol Lett*. 2016;12:1610-1614. doi:10.3892/ol.2016.4760

78. Younis M, Iqbal M, Shoukat N, Nawaz B, Watto FH, Shahzad KA. Effect of chemotherapy and radiotherapy on red blood cells and hemoglobin in cancer patients. *Sci Lett*. 2014;2:15-18.

79. Zeuner A, Signore M, Martinetti D, Bartucci M, Peschle C, De Maria R. Chemotherapy-induced thrombocytopenia derives from the selective death of megakaryocyte progenitors and can be rescued by stem cell factor. *Cancer Res*. 2007;67:4767-4773. doi:10.1158/0008-5472.CAN-06-4303

80. Iqbal M, Younis M, Shoukat N, et al. Hematological study of cancer patients with radio-chemotherapy. *Sci Lett*. 2015;3:75-79.

81. Braicu C, Buse M, Busuioc C, et al. A comprehensive review on MAPK: a promising therapeutic target in cancer. *Cancers (Basel)*. 2019;11:1618. doi:10.3390/cancers11101618

82. Dolcet X, Llobet D, Pallares J, Matias-Guiu X. NF-kB in development and progression of human cancer. *Virchows Arch*. 2005;446:475-482. doi:10.1007/s00428-005-1264-9

83. Campbell KJ, Tait S. Targeting BCL-2 regulated apoptosis in cancer. *Open Biol*. 2018;8:180002. doi:10.1098/rsob.180002

84. DiDonato JA, Mercurio F, Karin M. NF-kB and the link between inflammation and cancer. *Immunol Rev*. 2012;246:379-400. doi:10.1111/j.1600-065X.2012.01099.x

85. Xia L, Tan S, Zhou Y, et al. Role of the NFκB-signaling pathway in cancer. *Onco Targets Ther*. 2018;11:2063-2073. doi:10.2147/OTT.S161109

86. Liu F, Yang X, Geng M, Huang M. Targeting ERK, an Achilles' Heel of the MAPK pathway, in cancer therapy. *Acta Pharm Sin B*. 2018;8:552-562. doi:10.1016/j.apsb.2018.01.008

87. Kong D, Kim YK, Kim MR, Jang JH, Lee S. Emerging roles of vascular cell adhesion molecule-1(VCAM-1) in immunological disorders and cancer. *Int J Mol Sci*. 2018;19:1057. doi:10.3390/ijms19041057

88. Alexiou D, Karayiannakis AJ, Syrigos KN, et al. Serum levels of E-selectin, ICAM-1 and VCAM-1 in colorectal cancer patients: correlations with clinicopathological features, patient survival and tumour surgery. *Eur J Cancer*. 2001;37:2392-2397. doi:10.1016/s0959-8049(01)00318-5

89. Filippovich IV, Sorokina NI, Lisbona A, Chérel M, Chatal JF. Radiation-induced apoptosis in human myeloma cell line increases BCL-2/BAX dimer formation and does not result in BAX/BAX homodimerization. *Int J Cancer*. 2001;92:651-660. doi:10.1002/1097-0215(20010601)92:5<651::aid-ijc1248>3.0.co;2-7

90. Wunderlich R, Ernst A, Rödel F, et al. Low and moderate doses of ionizing radiation up to 2 Gy modulate transmigration and chemotaxis of activated macrophages, provoke an anti-inflammatory cytokine milieu, but do not impact upon viability and phagocytic function. *Clin Exp Immunol*. 2015;179:50-61. doi:10.1111/cei.12344

91. Sharma V, Anderson D, Dhawan A. Zinc oxide nanoparticles induce oxidative stress and genotoxicity in human liver cells (HepG2). *J Biomed Nanotechnol*. 2011;7:98-99. doi:10.1166/jbn.2011.1220

92. Kim M, Jeong H. Zinc oxide nanoparticles suppress LPS-induced NF-κB activation by inducing A20, a negative regulator of NF-κB, in RAW 264.7 macrophages. *J Nanosci Nanotechnol*. 2015;15:6509-6515. doi:10.1166/jnn.2015.10319

93. Kim SR, Jung YR, Kim DH, et al. Caffeic acid regulates LPS-induced NF-κB activation through NIK/IKK and c-Src/ERK signaling pathways in endothelial cells. *Arch Pharm Res*. 2014;37:539-547. doi:10.1007/s12272-013-0211-6

94. Min J, Shen H, Xi W, et al. Synergistic anticancer activity of combined use of caffeic acid with paclitaxel enhances apoptosis of non-small-cell lung cancer H1299 cells in vivo and in vitro. *Cell Physiol Biochem*. 2018;48:1433-1442. doi:10.1159/000492253

95. Sun J, Wang S, Zhao D, Hun FH, Weng L, Liu H. Cytotoxicity, permeability, and inflammation of metal oxide nanoparticles in human cardiac microvascular endothelial cells. *Cell Biol Toxicol*. 2011;27:333-342. doi:10.1007/s10565-011-9191-9

96. Moon MK, Lee YJ, Kim JS, Kang DG, Lee HS. Effect of caffeic acid on tumor necrosis factor-alpha-induced vascular inflammation in human umbilical vein endothelial cells. *Biol Pharm Bull*. 2009;32:1371-1377. doi:10.1248/bpb.32.1371

97. Nan W, Ding L, Chen H, et al. Topical use of quercetin-loaded chitosan nanoparticles against ultraviolet B radiation. *Front Pharmacol*. 2018;9:826. doi:10.3389/fphar.2018.00826

98. Wu Y, Zhang Q, Ruan Z, Yin Y. Intrinsic effects of gold nanoparticles on proliferation and invasion activity in SGC-7901 cells. *Oncol Rep*. 2016;35:1457-1462. doi:10.3892/or.2015.4474

99. Makena MR, Ranjan A, Thirumala V, Reddy AP. Cancer stem cells: road to therapeutic resistance and strategies to overcome resistance. *Biochim Biophys Acta Mol Basis Dis*. 2020;1866:165339. doi:10.1016/j.bbdis.2018.11.015

100. Chang L, Graham P, Hao J, et al. Cancer stem cells and signaling pathways in radioresistance. *Oncotarget*. 2016;7:11002-11017. doi:10.18632/oncotarget.6760

101. Santivasi WL, Xia F. Ionizing radiation-induced DNA damage, response, and repair. *Antioxid Redox Signal*. 2014;21:251-259. doi:10.1089/ars.2013.5668

102. Walle T, Martinez Monge R, Cerwenka A, Ajona D, Melero I, Lecanda F. Radiation effects on antitumor immune responses: current perspectives and challenges. *Ther Adv Med Oncol*. 2018;10:1-27. doi:10.1177/1758834017742575

103. Munshi A, Ramesh R. Mitogen-activated protein kinases and their role in radiation response. *Genes Cancer*. 2013;4:401-408. doi:10.1177/1947601913485414

104. Wei F, Yan J, Tang D. Extracellular signal-regulated kinases modulate DNA damage response—a contributing factor to

using MEK inhibitors in cancer therapy. *Curr Med Chem*. 2011;18:5476-5482. doi:10.2174/092986711798194388

105. Yan Y, Black CP, Cowan KH. Irradiation-induced G2/M checkpoint response requires ERK1/2 activation. *Oncogene*. 2007;26:4689-4698. doi:10.1038/sj.onc.1210268

106. Dainiak N. Hematologic consequences of exposure to ionizing radiation. *Exp Hematol*. 2002;30:513-528. doi:10.1016/s0301-472x(02)00802-0

107. Lin WS, Xu Y, Huang CC, et al. Toxicity of nano-and micro-sized ZnO particles in human lung epithelial cells. *J Nanopart Res*. 2009;11:25-39. doi:10.1007/s11051-008-9419-7

108. Subiel A, Ashmore R, Schettino G. Standards and methodologies for characterizing radiobiological impact of high-Z nanoparticles. *Theranostics*. 2016;6:1651-1671. doi:10.7150/thno.15019

109. Sanad F, Nabih S, Goda MA. A lot of promise for ZnO-5FU nanoparticles cytotoxicity against breast cancer cell lines. *J Nanomed Nanotechnol*. 2018;9:486. doi:10.4172/2157-7439.1000486

110. Namvar F, Rahman HS, Mohamad R, et al. Cytotoxic effects of biosynthesized zinc oxide nanoparticles on murine cell lines. *Evid Based Complement Alternat Med*. 2015;2015:593014. doi:10.1155/2015/593014

111. Ghosh M, Sinha S, Jothiramajayam M, Jana A, Nag A, Mukherjee A. Cyto-genotoxicity and oxidative stress induced by zinc oxide nanoparticle in human lymphocyte cells in vitro and Swiss albino male mice in vivo. *Food Chem Toxicol*. 2016;97:286-296. doi:10.1016/j.fct.2016.09.025

112. Pati R, Das I, Mehta RK, Sahu R, Sonawane A. Zinc-oxide nanoparticles exhibit genotoxic, clastogenic, cytotoxic and actin depolymerization effects by inducing oxidative stress responses in macrophages and adult mice. *Toxicol Sci*. 2016;150:454-472. doi:10.1093/toxsci/kfw010

113. Murad H, Alghamian Y, Aljapawe A, Madania A. Effects of ionizing radiation on the viability and proliferative behavior of the human glioblastoma T98G cell line. *BMC Res Notes*. 2018;11:330. doi:10.1186/s13104-018-3438-y

114. Zeng N, Hongbo T, Xu Y, Wu M, Wu Y. Anticancer activity of caffeic acid nbutyl ester against A431 skin carcinoma cell line occurs via induction of apoptosis and inhibition of the mTOR/PI3K/AKT signaling pathway. *Mol Med Rep*. 2018;17:5652-5657. doi:10.3892/mmr.2018.8599

115. Blanchard OL, Smoliga JM. Translating dosages from animal models to human clinical trials—revisiting body surface area scaling. *FASEB J*. 2015;29:1629-1634. doi:10.1096/fj.14-269043

116. Valic MS, Zheng G. Research tools for extrapolating the disposition and pharmacokinetics of nanomaterials from preclinical animals to humans. *Theranostics*. 2019;9:3365-3387. doi:10.7150/thno.34509

117. Shin JW, Seol IC, Son CH. Interpretation of animal dose and human equivalent dose for drug development. *J Korean Orient Med*. 2010;31:1-7.

118. Liao C, Jin Y, Li Y, Tjong SC. Interactions of zinc oxide nanostructures with mammalian cells: cytotoxicity and photocatalytic toxicity. *Int J Mol Sci*. 2020;21:6305. doi:10.3390/ijms21176305